INTERNATIONAL ATOMIC ENERGY AGENCY
UNITED NATIONS EDUCATIONAL, SCIENTIFIC AND CULTURAL ORGANIZATION
INTERNATIONAL CENTRE FOR THEORETICAL PHYSICS
I.C.T.P., P.O. BOX 586, 34100 TRIESTE, ITALY, CABLE: CENTRATOM TRIESTE

H4.SMR/650-14

Workshop on Three-Dimensional Modelling of Seismic Waves Generation Propagation and their Inversion

30 November - 11 December 1992

Point Source Moment Tensor Retrieval in Volcanic, Geothermal and Orogenic Areas by Complete Waveform Inversion

G.F. Panza (1,5), J. Sileny (2), P. Campus (1) R. Nicolich (3), G. Ranieri (4)

(1) Istituto di Geodesia e Geofisica, Università degli Studi di Trieste
Trieste, Italy

(2) Geophysical Institute, Czech. Academy of Sciences
Prague, Czechoslovakia

(3) Università di Trieste, Istituto di Miniere e Geofisica Applicata
Trieste, Italy

(4) Istituto Universitario Navale Napoli, Istituto di Oceanologia
Napoli, Italy

(5) International Centre for Theoretical Physics
Strada Costiera 11, 34100 Trieste, Italy

" JOURNAL OF APPLIED GEOPHYSICS "

Point source moment tensor retrieval in volcanic, geothermal and orogenic areas by complete waveform inversion

G. F. Panza[1,5], J. Šílený[2], P. Campus[1], R. Nicolich[3] and G. Ranieri[4]

[1] Universita` di Trieste, Istituto di Geodesia e Geofisica, Via dell'Universita` 7, 34123 Trieste, Italia
[2] Geophysical Institute, Czech. Acad. Sci., Bocni II, 14131 Praha 4, Czechoslovakia
[3] Universita` di Trieste, Instituto di Miniere e Geofisica Applicata, Piazzale Europa, 1, 34100 Trieste, Italia
[4] Istituto Universitario Navale Napoli, Istituto di Oceanologia, Via Acton 38, 80133 Napoli, Italia
[5] International Centre for Theoretical Physics, Via Beirut 7, 34100 Trieste, Italia

ABSTRACT.

Most of the seismicity which is characterising volcanic and geothermal areas is represented by relatively small events, which reflect the local answer to the global tectonic setting. Due to the strong seismic noise encountered in these areas, the source mechanisms of these events are usually very difficult to be studied by using standard techniques based on first arrivals, unless a very dense network of seismometers is available. When studying induced seismicity, a well known problem for geothermal areas, or volcanic events, it is highly desirable to treat a seismic source in a form a priori not restricted to a double couple since the mechanism may reflect the local conditions such as small-scale tectonics, fluid motion and man-made factors. The decomposition of the full (or unconstrained) moment tensor solution into a double-couple component (DC), a volumetric (V) component and a 'compensated linear vector dipole' (CLVD) component can indicate a measure of the relative influence of global tectonics and local effects. In orogenic areas, seismic events can be very strong, but the largest part of the earthquakes, which very likely reflect small scale complexities of the tectonic structure, is characterized by very small magnitudes. Therefore, the study of weak events is very important for many different purposes, and we apply here the inversion scheme of high-frequency seismograms, recorded by a local network, based upon the unconstrained moment tensor description.

A good knowledge of the structural model is a definite prerequisite to obtain reliable source information (moment tensor and time history not biased by propagation effects, even though not unique). For this reason we have inverted signals recorded in the Pozzuoli (Italy) area, using as input structure the model determined from a set of independent high-accuracy measurements. The inversion shows a first episode with the main peak centred around 0.6s, followed by another significant peak, with duration of 0.4s, centred at 2s, and by a final energy release extending for about 1.0s.

The procedure has been also applied to vertical component seismograms recorded in the Friuli (NE Italy) orogenic area in correspondence of the M = 2.9 event of December 27, 1987 and of two events of February 01, 1988, respectively with M = 3.2 and M = 3.6. The retrieved source mechanisms are generally in agreement with the distribution of the few first arrivals polarities available. The source time functions indicate possible multiple rupture processes also for relatively small magnitude events.

Keywords: inversion of waveforms, source mechanism and time function, mode summation, volcanic areas, mountain ranges.

Abbreviated title: Waveform inversion: moment tensor.

INTRODUCTION

Since the pioneering paper of Gilbert and Dziewonski (1975), who inverted free oscillation data to retrieve the source moment tensor of large earthquakes, many approaches have been proposed to study the earthquake source by inverting waveforms. The models of the source and the methods used differ greatly according to the purpose of the study and the data used. Here the seismograms observed in the stations of a local network (the distances between stations are roughly tens of kilometres) are considered. Our aim is to investigate weak events, therefore we concentrate on the point source approximation. The approach followed here has been developed by Šílený and Panza (1991) and Šílený et al. (1992) and resembles source studies performed by using teleseismic data (e.g., Mendiguren, 1977, Kikuchi and Kanamori, 1982, Trehu et al, 1981, Sipkin, 1982, Nabelek, 1984). However, our approach is more general than teleseismic studies, where either the hypocentre is fixed or is allowed to change in a given velocity model only. Both the depth of the source and the structural model, representing the area in which the event occurred, are permitted to vary within an a priori chosen range. This is done because the source depth strongly influences the wave-forms and, when body-waves arrivals are used for source-depth determinations, the resulting uncertainty is in general quite large; for similar reasons we have allowed changes in the structural parameters.

For seismic sources in volcanic and geothermal areas a "non double-couple" component cannot be excluded; the mechanisms of weak events in orogenic zones are believed to reflect small-scale complexities of the focal zone, therefore no a priori constraint of double couple mechanism is imposed. The source is described by the full (or unconstrained) moment tensor $M_{ij}(t)$, which can be decomposed in a volumetric component (V), representing an explosive or implosive movement, and in a deviatoric part, containing both the double couple (DC) and the compensated linear vector dipole (CLVD) components. This latter tensor, as the double couple, does not imply a change in the source volume and corresponds to three vector dipoles without moment, one of them is double in modulus with respect the others (Jost and Herrmann, 1989).

2. INVERSION OF OBSERVED WAVEFORMS

The method developed by Šílený and Panza (1991) and Šílený et al. (1992) has been applied to the inversion of several short period seismograms, recorded in volcanic and orogenic areas. The reconstruction of the V and CLVD components of the seismic moment tensor is particularly important for studying seismic sources in volcanic and geothermal areas. Since the accurate knowledge of the structural properties is a requirement for the correct retrieval of the V component of the moment tensor - moment tensor and time history not severely biased by propagation effects - (Šílený et al., 1992) we have inverted signals recorded in the Pozzuoli (Italy) area, using as input structure the elastic model determined from a set of independent high-accuracy measurements, and allowing only for variations of the quality factor Q in a given range.

2a. Structural model for the area of Pozzuoli

The potassic-type volcanic activity which occurred during Quaternary times, affecting large areas in the Campania region, has been attributed to tensional tectonics and to vertical faulting which were associated with the subsidence of the western margin caused by the opening of the Tyrrhenian basin and the uplift of the Apennine chain. The Phlegrean Fields are made up by a series of eruptive centres forming a caldera with a diameter of approximately 14 km. The magmatic activity is centered inside a carbonatic platform which outcrops not far from the area and is completely altered inside the caldera. The pre-caldera activity began in a marine environment and produced tuffs with sedimentary intercalation and lava domes. The post-caldera activity began 35000 years ago with the parossistic eruption of the Campanian ignimbrite (subaerial and chaotic tuffs, followed again by tuffs of submarine environment and local pyroclasts, C.N.R., 1987).

The P-wave velocity distribution has been defined, down to a depth of 3.5 km, using the data recorded inside the Pozzuoli Gulf during a high-resolution reflection seismic survey (Mirabile et al. 1989). From this depth and down to the Moho (about 26 km), deep seismic soundings data have been utilised (Ferrucci et al., 1989). For the upper

mantle the average velocity deduced from surface waves dispersion measurements has been used (Calcagnile and Panza, 1981). The density model has been defined from well measurements and gravimetric inversion (AGIP, 1987), while the Q distribution with depth has been taken as the variable structural parameter, in the definition of the structural interpolation range.

The multichannel reflection survey was carried out using a 24-channel streamer (25 m groups interval) and a 2-water gun array. More than 100 km of seismic lines were shot with either 1200 % or 2400 % coverage (25 or 12.5 m shot interval, see Fig. 2A). The 2 ms sampling rate and the wide band of the frequencies generated by the source allowed during processing the use of frequencies up to 120 Hz, with an excellent resolution and good penetration to the deepest part of the volcanic system. The acquisition and processing parameters adopted (deconvolution before stack, DMO, ω-x migration operator, sections with relative amplitude preservation, etc.) enhanced the potential of the methods applied to the understanding of the evolution of the caldera and of the actual volcanic risks. These data integrate the gravimetric and magnetic analysis made by AGIP (1987), subsequent to the prospecting activities carried out to determine the geothermal potential of the Phlegrean Fields.

The multichannel seismic survey has investigated volcanic formations and formations altered by an intense magmatic activity, where the S/N ratio is poor. Anyway it is possible to recognize variations in the petrophysical characteristics of the rocks and the influence of trapped fluids. Fig. 2B shows the seismic section (24 fold coverage) along the profile P1-P2, from the west (Baia) to the east (Nisida) crossing the central part of the gulf of Pozzuoli. This section shows reflections, often discontinuous, down to 2.2 s t.w.t. (3.0 to 3.5 km of depth), which can be related to fractured intervals characterised by the presence of hydrothermal products and accumulation of fluids (liquids and gases) seen as bright spots. The top of this metamorphosed interval is located at 1.5-1.7 s t.w.t. (horizon T in Fig. 2B and 2C). It is overlaid by units, seismically more transparent, probably pre-made of subacqueous to subaerial post-caldera volcanic products (tuffs). Also within these units it is possible to find trapped fluids as indicated by bright spots generated by water accumulations. The mostly submarine products of

the post-caldera activity top the dome-like structure (horizon C) and have a depocenter close to S.P. 200.

Correlation with the data from the wells Mofete1 and Mofete2, drilled by AGIP, can be established (Barberi et al., 1991). The post-caldera sequences are characterized by density values of 2.0-2.2 g/cm^3, interval velocity of only 1.7-2.2 km/s and thicknesses of approximately 0.7-0.8 km. The tuffs of the pre-caldera activity (T-C interval) have a density - measured in wells - of approximately 2.4 g/cm^3. The top of the thermo-metamorphic complex (T) delimits volcanoclastic recrystallized rocks with a density of 2.6 gr/cm^3 and velocities of 3.9 km/s. The properties of the seismic sequences seems to confirm the anomalous value (2.0-2.2) of the V_p/V_s ratio observed in a limited portion of the studied area in the neighbourhood of Pozzuoli (Aster et al., 1990, Scarpa, 1992). This high value may correspond to non compacted sediments or highly fractured rocks saturated by water. A dry fracturation mechanism in the generation of earthquakes requires a much lower V_p/V_s ratio (O'Connel and Budianski, 1976).

Fig. 2C shows the line PC-PD, from south to north, with a north-dipping horizon T. This structural trend may support the recent seismological studies of De Natale et al. (1990) who propose the existence of an elliptical fracture surface dipping towards the center of the caldera. This is confirmed by the distribution of the hypocentres which delimits the accumulation basin of the pyroclastic products. These earthquakes occur in correspondence with the borders of the newly formed and active parts of the caldera - near the top of horizon T which represents a brittle and resistant hinge marker at the top of a ductile interval. They can be generated by variations in the stress field which are caused by the same very deep and spatially extended magmatic source responsible for the horizontal and vertical deformations of the whole Phlegrean Field system (De Natale et al., 1990, 1992).

2b. Inversion of records in volcanic area

The P-wave model described in section 2a (Fig.1D) is quite reliable, while the V_p/V_s ratio is questionable and the high value estimated by Aster et al. (1990) and Scarpa (1992) may be not representative of the whole area. To be conservative, we have initially fixed the V_p/V_s ratio around $\sqrt{3}$ (Model POZZ1). Since the P-wave structure is well defined, a

single epicentral location of the analized event has been performed using only P-wave arrivals (Table I).

We have fixed Q_s=100 for the crust and 200 for the mantle (Q_p=2.2Q_s). The second extreme of the structural interpolation range has been obtained by varying only the Q factor (see Table V), the less known parameter, in the superficial layers. As second test, starting from the P-wave distribution of Model POZZ1, in the upper 3.5 km we have used a V_p/V_s ratio around 2.1, again using the two different Q distributions as extremes for the structural interpolation.

Four vertical-component signals have been analysed. They are indicated in the figures with the labels ST07, ST08, ST11, ST13. The data have been re-sampled to the time interval used to compute the base functions (0.0488 s) used in the inversion (Šíleny´ and Panza, 1991 and Šíleny´ et al., 1992), and successively low pass filtered. These signals have a very long duration which corresponds probably to a multiple event: therefore we have chosen to analyse the waveforms by selecting two different temporal windows. In the first test a D2 time window (Press et al., 1986) with duration of 5 s has been used. The base functions have been constructed with the epicentral determination and the origin time given in Table I, using the multimode method (Panza, 1985). On the basis of the focal depth estimates the depth range for the interpolation of the base functions varies from 0.5 to 1.9 km, with a step of 0.2 km.

Šíleny´ et al. (1992) have shown that the functions $M_{ij}(t)$ (i=j=1,2,3), representing the time dependence of the diagonal elements of the seismic moment tensor, can be affected by the a-priori assumptions made in the initial phase of the inversion procedure. These assumptions may cause these elements to be highly correlated and to have comparable amplitudes, i.e. to represent an apparent additional volumetric component. This volumetric component can easily be suppressed by substracting, at each time t, the average $(M_{11} + M_{22} + M_{33})/3$ from the diagonal elements M_{ii}. The functions obtained after the subtraction can be called *reduced functions* $m_{ij}(t)$. The reduced functions $m_{ij}(t)$ reproduce very closely the true source duration. Furthermore, the same authors have shown that the use of completely independent time histories for each component of the moment tensor may give rise to physically questionable results, like, for instance, correlation between all the $M_{ij}(t)$ traces, and reverse motion.

The correlation existing between the $M_{ij}(t)$ traces suggests to assign a joint time function to all the six components and to find six scalar multipliers, λ_{ij} (i,j = 1,...3 and $\lambda_{ij}=\lambda_{ji}$), the product of which with the joint time function would approach the reduced functions $m_{ij}(t)$ as closely as possible. To reject reverse motion during the rupturing process the additional condition of non negative joint time function is imposed. The joint time function reproduces the source time function, i.e. the shape and the time duration of the energy release, the multipliers λ_{ij} are the amplitudes of the moment tensor, constant for all the rupture process, and provide the average mechanism of the event. The joint time function gives, when multiplied by the λ_{ij}, the reduced functions $m_{ij}(t)$.

If the range of structural models used in the inversion differs greatly from the reality the amplitudes of the spurious signals in $M_{ij}(t)$ can be large enough to mask entirely the moment tensor time function corresponding to the real source. There are two ways to remove these spurious signals. The constraint of a non-volumetric source can be imposed in the inversion. This gives only an approximate agreement of the synthetic seismograms with the records, but the time functions of the moment tensor reflect the source characteristics quite well. However, on the basis of our experience, it seems to be more appropriate to solve the inverse problem for a general moment tensor source and to remove a posteriori the volumetric part from the solution of this unconstrained problem. With the latter procedure the time function of the moment tensor can be well reconstructed both in duration and in shape.

With the data shown in Fig. 3A (solid line) a set of numerical experiments has been performed with unconstrained moment tensor and for various lengths of the functions $M_{ij}(t)$. The first inversion of the records, with maximum frequency content of 10 Hz, has been performed with the source time function parametrized by 20 time-delayed triangles (Δt = 0.0488 s) with half-width $\Delta\tau = \Delta t$. It results in the synthetic seismograms shown in Fig. 3A as dashed lines. The obtained $M_{ij}(t)$ and the deviatoric components $m_{ij}(t)$ are shown in Fig. 3B as solid and dashed lines, respectively. The volumetric component is about 8% of the total moment tensor. Introducing the scalar multipliers λ_{ij} we can get the joint time function shown in Fig. 3C. The first part of the signals seems to be generated by an initial very small energy release at about 0.1 s, with duration of 0.3 s, followed by the main energy

release, centred around 0.6 s, with duration of 0.1 s. Two smaller energy releases appear around 0.8 s and 1.0 s.

The average mechanism and that deduced from the first significant peak of the $m_{ij}(t)$ are similar and in accord with the distribution of P-wave polarities, determined using the program written by Brillinger et al.(1980) (Figs. 3D and 3E).

The analysis of the data filtered to 5 Hz (Fig. 4A) confirms that the first small energy release, with duration of 0.3 s, starts at 0.1 s and is followed by the main energy release centred around 0.6 s (Fig. 4C). The average mechanism (Fig. 4D), coinciding in this case with that obtained from the first peak of the $m_{ij}(t)$, is in agreement with that obtained from the inversion of the data filtered at 10 Hz.

Let us indicate now the source depth with the variable X and let us introduce the parameter Y ($0 \le Y \le 1$) to represent the different structural models within the range defined by the extreme models A and B, choosen a priori. When Y=0 the structure used to compute the base functions is A, when Y=1 the considered structure is B. The structures corresponding to the values of the variable Y in the range [0,1] are more similar to A if Y<0.5, more similar to B if Y>0.5. In the course of the inversion intermediate values of the parameters X and Y are computed, incrementing the initial values usually taken equal to 0.5 with steps chosen *a priori*. The retrieved values of X and Y are, in the first test (cut off frequency at 10 Hz), X=0.97 and Y=0.33, in the second one (cut off frequency at 5 Hz) X=0.84 and Y=0.99. This confirms that the event is very shallow, as evidenced in the preliminary hypocentral determination (see Table I). The great variation of the parameter Y, indicates a low sensitivity of the data set to the Q structure, but allows us to exclude, in the parametrization we have chosen, high Q values (Q = 100) in the upper crust.

The second time window applied to the data has a length of 10 s. The waveform reconstruction of the data filtered to 10 Hz is shown in Fig. 5A. In the joint time function (Fig. 5C) it is possible to recognize the multiple process which characterizes the energy release. The first episode is the same singled out using the 5 s time window, with the main peak centred around 0.6 s, followed by others significant peaks, with duration of 1.6 s, centred at 2 s, and by a final energy release extending for about 1.8 s.

The average mechanism (Fig. 5D) is essentially characterized by very similar dip and strike angles, but opposite slip angle with respect to that obtained by using the shorter time window. This fact shows an important aspect of the non-uniqueness of the inverse fault plane solution, based on waveform inversion, already recognized by Bukchin (1989). In fact, it is possible that equivalent minima (in the L_2-norm of the difference between the observed records and the synthetic seismograms) are reached considering signals shifted by about π: this is due to the allowed size of the time shifts in the inversion. This is only an apparent shortcoming of our procedure, since the use of the highly reliable P-wave polarities makes it possible to choose he proper slip angle. In the case we are treating here, the mechanism in agreement with the reliable polarities is that deduced from the inversion with the 5 s time window.

The mechanism obtained from the first significant peak of the $m_{ij}(t)$ is shown in Fig. 5E. One fault plane has the same orientation as the average mechanism, while the other one is rotated by about $\pi/2$. The difference between the two mechanisms suggests that the source process changes with time, the initial motion being of thrust type, while the main energy release takes place as a strike-slip type. The analysis of the data filtered to 5 Hz (Fig. 6A) shows that to fit the data with a lower frequency content the first three energy releases retrieved in the inversion of the high frequency records are essentially sufficient (Fig. 6C).

The average mechanism (Fig. 6D) is characterized by very similar dip and strike angles, but with a slip angle opposite to that obtained in the test with the high frequency data. This is in agreement with that obtained in the inversion of the earlier part of the signals. On the basis of the few reliable P-wave polarities, the accepted mechanism is that deduced from the low frequency data. The information contained in the mechanism obtained from the first significant peak of the $m_{ij}(t)$ is shown in Fig. 6E and maintains a similar distribution of compressions and dilatations, but only one plane orientation.

The values of X and Y for the data filtered to 10 Hz and to 5 Hz are respectively X=1.4, Y=0.74 and X=1.9, Y=0.05, indicating a very low resolution of the Q model and a quite significant variation of the source depth. Thus, the radiation at low frequency seems to come from a depth greater than that generating the high frequency data.

The value of M_0 can be defined as the product of the scalar moment, obtained from the eigenvalues of the moment tensor matrix, with the area under the source time function. In this case it is equal to 1.8 10^{10} Nw m. This value, following the relation, between the magnitude M and the seismic moment M_0, M=2/3 log M_0-6. given by Hanks and Kanamori (1979), is in good agreement with the estimated magnitude (1.1) of the event.

The volumetric part V, in the various inversion experiments, is always relevant and varies from a minimum of 7% to a maximum of 28% of the total moment tensor. The large variation of the volumetric part is an experimental confirmation of what was described in section 2b. However, our inversion scheme, even if it does not allow at present the retrieval of the correct size of the V component, is suitable to monitor its variation with time (i.e. from one earthquake to another one) and therefore can supply a useful tool for monitoring fluid action in volcanic and geothermal areas.

In a portion of the area under study, for the upper 3.5 km a V_p/V_s ratio of about 2.1 has been proposed by Aster et al. (1990) and Scarpa (1992). Therefore, we have repeated the inversion experiments described above with new extremes for the structural interpolation range satisfying this requirement. The results are similar to those obtained in the previous tests. When using a D2 time window with duration of 5 s (Figs.7A-E) a first little energy release, centred around 0.1 s, is followed, after 0.4 s, by the main peak. Two final peaks are centred around 0.7 s and 0.9 s. The values of X and Y are respectively 0.9 and 0.62 and confirm that the structure preferred in the inversion does not have a high Q. The average mechanism, equal in this case to that obtained from the first significant peak of the $m_{ij}(t)$, is of the strike-slip type showing a very similar dip and strike angles, but opposite slip angle with respect to that obtained in the corresponding test with the V_p/V_s ratio of $\sqrt{3}$. With a D2 time window of duration of 10 s (Figs.8A-E) the main energy release is confined to the first 2 s. Again the average mechanism is equal to that obtained from the first significant peak of the $m_{ij}(t)$ functions and is characterized by reverse slip, with respect to the test with the V_p/V_s ratio of $\sqrt{3}$. The values of X and Y are, respectively, 0.93 and 0.8, in agreement with the results obtained with the D2 time window of 5.4 s.

The low-pass filtered data yield, for $V_p/V_s = \sqrt{3}$, essentially the same results and therefore are not presented here.

The presence of a CLVD component can be an artefact generally due to a misinterpretation of multiple ruptures as single events (Julian and Sipkin, 1985) or to systematic errors in the determination of the moment tensor produced by lateral heterogeneity in the earth structure (Frohlich et al., 1989) but sometimes can be also the effect of rapid opening of cracks under high fluid pressure (Julian and Sipkin, 1985). In the performed tests the structural model is reliable, relevant lateral variations seem to be absent and the source point approximation is reasonable, because the magnitude of the analysed event is small. Therefore, the presence of the CLVD component (from 20% up to 30%) could be effectively caused by crack opening due to fluid motion. Even if the real size of the CLVD component can hardly be determined, very useful informations about change in the pattern of fluid motion can be obtained by the variation in time (different earthquakes) of the CLVD component, which can be easily monitored with our method.

3c. Inversion of records in orogenic areas

In orogenic areas the DC model for seismic sources seems to be a satisfactory model, thus an accurate structural model is not critical, and an average model obtained from the inversion of seismological data can be sufficient. As an example, vertical short-period seismograms, proportional to the ground velocity recorded in the Friuli area (Italy), during the earthquake of December 12, 1987 and two earthquakes of February 1, 1988, have been inverted. The data have been re-sampled to the time interval used to compute the base functions (0.0488 s), and subsequently low pass filtered. The stations coordinates are given in Tables II, III, IV. For the hypocentral location we have the three independent estimates listed in Table II corresponding to the one-dimensional structural models FRIUL7A (model A) (Panza and Suhadolc, 1987), FRIUL7W (model W) (Mao and Suhadolc, 1992) and O.G.S. (Anonymous, 1987).

For the event of December 12, 1987 the latitude and longitude values obtained using the O.G.S. model differ by about 0.4 km and 0.2 km from those of the model A, and by about 1.5 km and 1.0 km from those of the model W. The source depth, for the model O.G.S. differs

from that for model A by about 0.2 km, and by about 2.4 km from that for model W. Since we have chosen as extreme structures the models A and W (Fig. 1A and Fig. 1B), a first set of tests has been made by assuming the epicentral distances and the origin time obtained from the model W, while in a second set of tests the epicentral determinations and the origin time obtained from the structural model A have been used. On the basis of the depth estimates shown in Table II the depth range for the interpolation of the base functions varies from 6 to 10 km. With the depth spacing of 0.5 km, a set of numerical experiments has been performed both with unconstrained moment tensor and with the non-volumetric constraint, and then for various duration of the $M_{ij}(t)$ functions.

In the first test the analysed signals have a length of 5.4 s, obtained by applying to the 10 Hz data a D2 window (Fig. 9A, solid lines). The stations considered are Monte Prat (MPRV), Bordano (BOOV), Montereale Valcellina (RCLV), Bernadia (BADV) and Zoufplan (ZOUV). The base functions have been constructed with the epicentral determination and the origin time deduced from the model W. The inversion, performed with the unconstrained moment tensor formalism and the source time function parametrized by 20 time-delayed triangles (Δt = 0.0488 s) with half-width $\Delta\tau = \Delta t$, gives the synthetic seismograms shown in Fig 9A as dashed lines. The focal depth is determined to about 8.0 km and the final value of Y is 0.97, which implies that a structure very near to the W model seems to be the most appropriate one-dimensional representation of the area under study. The $M_{ij}(t)$ and the deviatoric components $m_{ij}(t)$ are shown in Fig. 9B as solid and dashed lines respectively. The volumetric component (V) is practically absent. Introducing the scalar multipliers λ_{ij}, defined in section 2a, we can get the joint time function shown in Fig. 9C; the earthquake seems to be characterized by two main episodes of release of energy: the first lasting for about 0.5 s and the second around 0.8-0.9 s. On the basis of the results discussed in section 3.2 of Sileny et al. (1992), the second energy release can be an artefact introduced by the use of a not completely adequate structural model, but, as will be shown by the analysis of data low-pass filtered at 5 Hz, it can also bear some real information on the source process.

The distribution of the few available first-arrival polarities (open and solid circles in Fig. 9D) is consistent with the average mechanism

obtained (Fig. 9D, shaded areas). The mechanism corresponding to the first peak of the $m_{ij}(t)$ is shown in Fig. 9D. It is very similar to the average one. The test performed by using the epicentral distances and the origin time obtained from the model A gives results in agreement with the previous ones (Fig. 10A-D). The structural parameter Y is 0.89, i.e. a structure near to the model W is selected also in this case. The retrieved depth is about 7.5 km. The joint time function (Fig. 10B) has a duration similar to that shown in Fig. 9C. In this case the first rupturing episode seems to be formed by three distinct energy releases, centred at about 0.1 s, 0.3 s and 0.55 s. The average mechanism and that deduced from the first peak of the $m_{ij}(t)$ functions are very similar and in agreement both with the polarity distributions and with the mechanisms shown in Fig. 9D and Fig. 9E. The only difference is an increase of the CLVD component from about 5% to about 10% (compare Fig. 10C and Fig. 10D with Fig. 9C and Fig. 9D).

On the basis of the results obtained so far, we have decided to perform some stability tests by using only the base functions computed with the origin time and the epicentral distances deduced from the model W. Some of these tests have been performed by enhancing with suitable weights the contribution of the normal equations (see equation 10 in Sileny et al., 1992) referred to the records with lower amplitudes. The waveform reconstruction improves for the enhanced signals, while it becomes poorer for the records with the largest amplitudes. Moreover the average mechanism and that deduced from the first peak of the $m_{ij}(t)$ functions are in disagreement with the polarity distribution. This is not surprising because the amplitudes recorded in the distant stations are ten times lower than those recorded in the near stations. When the 'distant' amplitudes are made comparable in the resolution of the normal equations the consequent amplification of the noise contained in the records can strongly contaminate the inversion. We have also inverted low pass filtered data to see if and how the rupture process changes when it is seen at lower frequencies. Using data low-pass filtered at 5 Hz, the depth is retrieved at about 9.7 km and the value of the structural parameter Y is 0.9, again very near to the structure W (Fig. 11A-C). In this case we have fixed Δt = 0.0976 s. In the joint time function (Fig. 11B) two relatively broad peaks are detected at about 0.4 s and 0.8 s. The comparison with the joint time function of Fig. 9C and Fig. 10C shows that the low frequency records pratically do not

contain information about the initial episode centred at about 0.05-0.1 s. In fact this episode is characterized by a duration which is shorter than the minimum period contained in the 5 Hz low-pass filtered data.

On the basis of the experience made with the synthetic data, the presence of the broad peak centred at about 0.8 s can indicate that this energy release is not completely an artefact due to the structural inadequacy. In spite of the large difference in the time history, the resulting average mechanism preserves the strike-slip characteristic and is still in agreement with the few available P-wave polarities and with the average focal mechanism obtained from the high-frequency data. Further tests have been performed by varying the length of the inverted signals. Stability in the retrieved depth, in the structural parameter and in the planes orientation deduced from the first peak of the $m_{ij}(t)$, characterizes all the tests. The joint time function undergoes some modifications, but the character of two distinct energy releases is preserved. The first significant peak of the $m_{ij}(t)$, gives the same information obtained in the analysis of the high frequency records.

The two events of February 1, 1988, despite of the small difference in the epicentral locations (about 4 km in latitude and 6 km in longitude) and in the origin time (about 4 s) appear to be characterized by different source mechanisms and depth. In the analysis of the first event of February 1, 1988 the latitude and longitude values obtained using the O.G.S. model differ respectively by about 3.3 km and 8.5 km from those obtained both using the model A and the model W. This is due in part to the elimination, when using the structural models A and W, of a P-wave arrivals reading, probably wrong and used in the O.G.S. model. The source depths obtained with the models O.G.S. and A respectively, differs by about 1.5 km. This difference is of about 0.8 km when the results obtained with the models O.G.S. and W are compared.

Four vertical component signals, Buia (BUAV), Bernadia (BADV), Paularo (PLRV) and Zoufplan (ZOUV), with the maximum frequency content equal to 10 Hz, have been analysed. The inversion, performed with the unconstrained moment tensor formalism and the source time function parametrized by 20 time-delayed triangles with half-width $\Delta\tau$=0.0488 s, gives the synthetic seismograms shown in Fig 12A. The event seems to be characterised by a first energy release, with duration of 0.4 s, followed about 0.2 s later by a second smaller episode with

duration of 0.2 s (Fig. 12C). The average mechanism and that deduced from the first significant peak of the $m_{ij}(t)$ are similar: this means that the initial and main energy releases did take place with the same mechanism (Figs. 12D and 12E). The retrieved value of the parameter Y is 0.9, that is, also for this event, a structure very near to model W seems to be the most appropriate. The hypocentral depth is retrieved around 4.6 km.

In the inversion of the signals filtered at 5 Hz two parametrizations of the source have been performed: in the first one the triangles have a half-width of 0.1 s (that is two times the sampling step of the data), which permits the reconstruction of waveforms with a maximum frequency around 5 Hz. In the second one the half-width of the triangles is of 0.15 s, which permits the reconstruction of waveforms with a maximum frequency around 3 Hz. The waveform reconstruction is satisfactory in both cases (Figs. 13A and 14A) and the corresponding processes of energy release are characterized by two main peaks centred around 0.2 s and 0.6 s (Figs. 13C and 14C). These results are in agreement with those obtained with the inversion of the 10 Hz data. The average and initial mechanisms obtained with the triangles of half-width 0.15 s (Figs. 14D and 14E) are very similar to those obtained in the 10 Hz inversion, while those obtained with the triangles of half-width 0.1 s (Figs. 13D and 13E) give a mechanism which is characterized by very similar dip and strike angles, but opposite slip angle. The mechanism in agreement with the reliable polarities is that deduced from the inversion with the triangles of half-width equal to 0.1 s. The retrieved depth for the first parametrization is equal to 5 km, while for the second one it is equal to 4.3 km. The structural parameter has the value Y=0.54 in the first parametrization and Y=0.43 in the second one. Therefore structural models closer to W than to A seems to be the most appropriate.

The value of the seismic moment M_0 obtained from the inversion of the data filtered at 10 Hz is equal to $3.2\ 10^{13}$ Nw m, which corresponds to a magnitude 3 (Hanks and Kanamori, 1979), and is in good agreement with the measured (M=3.2) one. The CLVD component in all the performed tests varies from 8% to 30%.

For the second event of February 1, 1988 the latitude and longitude values obtained using the O.G.S. model differ by about 1.2 km and 1.3 km from those obtained from the models A and W, respectively.

For the source depth there is a very significant difference both between the results obtained using the models O.G.S. and A - about 8.3 km - and between the results obtained using the model O.G.S. and W - about 8.1 km.

Five vertical component signals, Bordano (BOOV), Buia (BUAV), Bernadia (BADV), Paularo (PLRV) and Zoufplan (ZOUV), with the maximum frequency content equal to 10 Hz, have been analysed. In view of the extension in time of the signals (about 10 s) we have parametrized the source with a relatively large duration, which can be obtained either by using a large number of triangles with the minimum half-width (equal to the sampling step of the data), or by using a smaller number of triangles with a half-width larger than the minimum one. On the basis of our experience, the use of a large number of triangles with the minimum half-width yields a good fit of the signals but an unrealistic reconstruction of the time history of the event. This is obviously due to the fact that the data set is not sufficient to resolve the fine details of the rupture process. Therefore we have chosen to parametrize the source with a limited number of triangles (ten) of half-width equal to three times the sampling step of the data. The results are shown in Figs. 15A and 16A.

In the first experiment (Fig. 15A) the base functions for all the stations have been computed with the extreme structural models A and W. The waveform reconstruction is satisfactory, with the exception of the signal corresponding to the station of Paularo. To improve the reconstruction of this signal we have computed the pertinent base functions using two new extreme structures, A' and W', which differ from the A and W in the first layers in which the sedimentary part has been suppressed.

The results of the new inversion are shown in Fig. 16A: the situation is partially improved for PLRV, remaining essentially unaltered for the other signals. From both inversions it appears that there is a single energy release extended in time, with a duration of about 1 s (Figs. 15C and 16C). In this case and in the previous one the average mechanism and that deduced from the first significant peak of the $m_{ij}(t)$ are obviously coincident and are in accord with the polarity distribution (Figs. 15D and 16D). In the first case the retrieved depth is about 2 km and the value of Y is 0.94, in the second the depth is again about 2 km and the value of Y is 1. Therefore this event is much shallower than the

previous one and probably located in the very attenuating sedimentary part of the structure, as suggested also by the spectral analysis of the signals which shows the major amplitudes in correspondence of relatively low frequencies (3-4 Hz).

The analysis of the data filtered at 5 Hz gives again a satisfactory waveform reconstruction for all the signals, apart the station of PLRV, for base functions computed with the extreme structural models A and W (Fig. 17A) for all the stations. When for the station of PLRV the base functions are computed with the two new extreme structures A' and W' the situation improves significantly (Fig. 18A). In both cases the energy release seems to be split into three distinct episodes separated respectively by 0.8 s). Each of them has a duration of 0.3 s (Figs. 17C and 18C). The average mechanism and that deduced from the first significant peak of the $m_{ij}(t)$ have similar fault-plane orientation (Figs. 17D-E and 18D-E). These mechanisms are different (one plane is rotated of about $\pi/2$) from that obtained from the inversion of the data filtered at 10 Hz. In these tests the hypocentre is located at 0.8 km and 1.0 km respectively, which confirms the rather shallow hypocenter inverted from the data filtered to 10 Hz. The parameter Y (structural resolution) varies between 0.5 and 0.6; therefore, as in the case of the first event of 1 February, 1988, a structural model closer to W than to A seems to be appropriate.

The overall fit of the traces is less satisfactory than for the other studied event. One possible explanation is the relatively large size of the considered event, M = 3.6, for which the point source approximation in space may be not adequate, mainly when considering frequencies above 5 Hz. This can justify the difference in the mechanisms obtained from the inversion of the data filtered at 10 Hz and at 5 Hz, which can probably be associated to different points of the fault, one located at a depth of about 2 km, the other one much shallower, around 1 km.

The value of the seismic moment M_0 obtained from the inversion of the data filtered at 10 Hz is equal to $1.3\ 10^{15}$ Nw m, which corresponds to a magnitude 4 (Hanks and Kanamori, 1979). In all the performed tests the CLVD component varies from 10% to 20%. The presence of a relevant CLVD component in the last two events, can be due both to the effect of the use of a structural range not very appropriate and to the not completely satisfactory approximation of the

seismic source by means of a point source, since the magnitude of both events is greater than 3.

CONCLUSIONS

The method of waveform inversion developed by Šílený and Panza (1991) and Šílený et al. (1992) allows us to retrieve the moment tensor of a point source as a function of time. In comparison with already existing similar approaches it has two advantages: (1) it allows to vary the structural model during the inversion; this is accomplished by interpolation between the base functions a priori computed for two structural models which can be assumed as acceptable extremes for the region under study; (2) it allows to change the focal depth in the course of the inversion, by means of a linear interpolation, with variable spacing, between the base functions a priori computed for a set of different depths.

The method provides a good estimate of the complete seismic moment tensor when the structural model is determined with sufficient reliability. An unreliable model gives rise to a spurious volumetric component which must be removed. The remaining deviatoric part of the moment tensor contains valid information about the source mechanism.

The inversion of the records generated by relatively small events in tectonic and volcanic areas indicates that even events of small size can have a relatively complex rupture mechanism. The inversion method is particularly suitable for studying, in a given volcanic or geothermal area, the variation from one event to another of the V and CLVD component of the moment tensor. This has obvious implications for the monitoring of fluid motion, which may accompagny the opening of cracks (CLVD component).

ACKNOWLEDGEMENTS

We thank Dr. M. Russi of Osservatorio Geofisico Sperimentale, Trieste, for supplying the experimental data of the Seismological network, supported by the Regione Friuli-Venezia Giulia and Dr. F. di Cesare of AGIP, Milano, for the data collected in the Pozzuoli area. We acknowledge financial support from GNDT (CNR contracts ris.# 90.01007.54 and 91.02539.54) and MURST (40% and 60% Funds). Special thanks go to ENEA for allowing us the use of the IBM 3090E of the Computer Centre ENEA INFO BOL. The research has been carried out in the framework of the activities planned by the Central European Initiative - Committee for Earth Sciences, and is a contribution of the ILP Task Group II-4.

REFERENCES

AGIP (1987). Geologia e geofisica del sistema geotermico dei Campi Flegrei. MESG-SERG, S. Donato Milanese, 19 pages.

Aki K. and Richards P.G. (1980). Quantitative seismology, Freeman and co., San Francisco.

Anonymous, (1987). Bollettino della rete sismometrica dell'Italia nord orientale. Osservatorio Geofisico Sperimentale, Trieste.

Aster, R.C., Meyer, R.P., De Natale, G., Zollo, A., Martini, M., Del Pezzo, E., Scarpa, R. and Iannaccone, G. (1990). Seismic investigation of the Campi Flegrei caldera. In: Volcanic Seismology, Proc. Volcanol. Series III, Springer-Verlag, Heidelberg.

Barberi, F., Cassano, E., la Torre, P and Sbrana, A. (1991). Structural evolution of Campi Flegrei caldera in light of volcanological and geophysical data. J. Volc. Geother. Res., 48:33-49. C.N.R., 1987. Phlegrean Fields.

Brillinger D.R., Udais A. and Bolt B.A. (1980). A probability model for regional focal mechanism solutions. Bull. Seismol. Soc. Am., 70:149-170.

Bukchin B. (1989). On estimation of source parameters from sourface waves data for poorly known medium. AGU, Physics of the Solid Earth, 25, 9.

Calcagnile G. and Panza G.F. (1981). The main characteristics of the litosphere-astenosphere system in Italy and surronding regions. Pure Appl. Geophys., 119:865-879.

CERN (1985). Computer Centre Program Manual, CERN, Geneve.

C.N.R. (1987). Phlegrean Fields, M. Rosi and A. Sbrana (eds.). Quaderni de "La Ricerca Scientifica", 9, 114:1-75.

De Natale G., Ferraro A., Virieaux J., Esposito T. and Zollo A. (1990). Analisi dei meccanismi focali dello sciame sismico del 1/4/84 ai Campi Flegrei: implicazioni vulcanologiche. Atti IX Convegno G.N.G.T.S., in press.

De Natale G., Pingue, F., Allard, P. and Zollo, A. (1992). Geophysical and geochemical modelling of the 1982-1984 unrest phenomena at Campi Flegrei caldera (southern Italy). J. Volcanol. Geotherm. Res., 48:199-222.

Ferrucci, F., Hirn, A., Gaudiosi, G., Luongo, G., Mirabile, L. and Pino, N.A. (1989). Seismic detection of a major Moho upheaval beneath the Campania volcanic area (Neaples, Southern Italy). Geophys. Res. Letters, 16, 11:1317-1320.

Frohlich C., Riedsel, M. A. and Apperson, K. D. (1989). Note concerning possible mechanisms for non-double couple earthquakes sources. Geophys. Res. Lett., 16:523-526.

Gilbert F. and Dziewonski A.M. (1975). An application of normal mode theory to the retrieval of structural parameters and source mechanisms from seismic spectra. Phyl. Trans. Roy. Soc. London, A278:187-269.

Hanks T.C. and Kanamori H. (1979). A moment-magnitude scale. J. Geophys. Res., 84:2348-2350.

Hartzell S.H. and Heaton T.H. (1983). Inversion of strong ground motion and teleseismic waveform data for the fault rupture history of the 1979 Imperial Valley, California earthquake. Bull. Seismol. Soc. Am. 73:1553-1583.

Jost M.L. and Herrmann R.B. (1989). A student's guide and Review of Moment Tensors. Seismol. Res. Letters, 60:36-57.

Julian, B. R. and Sipkin, S. A. (1985). Earthquake processes in the Long valley Caldera Area, California. J. Geophys. Res., 90:11155-11169.

Kikuchi M. and Kanamori H. (1982). Inversion of complex body waves. Bull. Seismol. Soc. Am., 72:491-506.

Mao W.J. and Suhadolc P. (1992). Simultaneous inversion of velocity structures and hypocentral locations: application to the Friuli seismic area NE Italy, Pure Appl. Geophys., in press.

Mendiguren J. (1977). Inversion of surface wave data in source mechanism studies. J. Geophys. Res., 82:889-894.

Mirabile, L., Nicolich, R., Piermattei, R. and Ranieri, G. (1989). Identificazione delle strutture tettono-vulcaniche dell'area Flegrea: sismica multicanale nel golfo di Pozzuoli. Atti VII Convegno G.N.G.T.S., Vol. II:829-838.

Nabelek J.L. (1984). Determination of earthquake source parameters from inversion of body waves. Ph.D. Thesis, Massachusetts Inst. of Technology.

O'Connel, R. and Budianski B. (1976). Seismic velocities in dry and saturated cracked solid. J. Geophys. Res., 79:5413-5426.

Ohlson A.H. and Apsel R.J. (1982). Finite faults and inverse theory with applications to the 1979 Imperial Valley earthquake. Bull. Seismol. Soc. Am. 72:1969-2001.

Panza G.F.,(1985). Synthetic seismograms: the Rayleigh waves modal summation, J. Geophys., 58:125-145.

Panza G.F. and Suhadolc P. (1987). Complete strong motion synthetics. In: Strong motion synthetics (Bolt A.B. ed.), Academic Press, Orlando, 135-204.

Press W.H., Flannery B.P., Teukolsky S.A. and Vetterling W.T. (1986). Numerical Recipes, Cambridge University Press, Cambridge.

Robinson E.A. (1967). Multichannel Time Series Analysis with Digital Computer Programs, Holden Day, San Francisco.

Rosi M. and Sbrana A.(eds.). Quaderni de "La Ricerca Scientifica", CNR-Rome, 114, 9:1-175.

Scarpa, R. (1992). Seismic tomography and modeling of complex geological structures, this volume.

Šílený J. and Panza G.F. (1991). Inversion of seismograms to determine simultaneously the moment tensor components and source time function for a point source buried in a horizontally layered medium. Studia geoph. geod. 35:166-183.

Šílený J., Panza G.F and Campus P. (1992). Waveform inversion for point source moment tensor retrieval with variable hypocentral depth and structural model. Geophys. J. Int., 109:259-274.

Sipkin S.A. (1982). Estimation of earthquake source parameters by inversion of waveform data: synthetic waveforms. Phys. Earth Planet. Int., 30:242-259.

Trehu A.M., Nabelek J.L., and Solomon S.C. (1981). Source characterization of two Reykjanes Ridge earthquakes: surface waves and moment tensors; P wave forms and nonorthogonal nodal planes. J. Geophys. Res., 86:1701-1724.

FIGURE CAPTIONS

Fig. 1. Structural models, for the Friuli and Pozzuoli regions, used in this study. A model FRIUL7A (Friuli), B model FRIUL7W (Friuli), C model FRIUL7R (Friuli), D model POZZ1 (Pozzuoli).

Fig. 2. Pozzuoli area. A: seismic lines along which the seismic recordings have been performed (24 fold coverage); B: seismic section (24 fold coverage) along the profile P1-P2, from the west (Baia) to the east (Nisida) crossing the central part of the gulf of Pozzuoli: **C** possible top of pre-caldera products, **I** lavas and hydrothermal products, **B1,B2,B3** trapped fluids, **T** top of the thermo-metamorphic complex, the arrow indicates the way of intrusion of the most recent volcanic products; C: seismic section (24 fold coverage) along the line PC-PD, from south to north: **C** possible top of pre-caldera products, **I** lavas and hydrothermal products, **B4,B5,B6** trapped fluids, **T** top of the thermometamorphic complex, **K** top of the carbonates, the arrow indicates the direction of intrusion of the most recent volcanic products

Fig. 3. Inversion of waveforms of the event of November 8, 1986, recorded, in the Pozzuoli area, by four local stations (ST07, ST08, ST11, ST13) respectively at epicentral distances of 1.6, 2.7, 6.7 and 4.2 km, and azimuths of 255°, 10°, 121° and 69°. Origin time: 04:20:48.16; epicentral coordinates: 40° 49.68'N, 14° 05.52'E. The V_p/V_s ratio used in the first 3.5 km of the extreme structures is around $\sqrt{3}$. A: data (solid lines) and synthetic seismograms (dashed lines) obtained with the unconstrained inversion with the base functions constructed in the depth interval 0.5-1.9 km and a spacing of 0.2 km; data and synthetic seismograms are truncated with a D2 window with a duration of 5 s; B: $M_{ij}(t)$ functions (solid lines) obtained with the unconstrained inversion and their reduced values $m_{ij}(t)$ (dashed lines); C: joint time function constrained between 0 and 1, in the right upper part is indicated the scaling factor; D: average focal mechanism obtained from the six multipliers λ_{ij} (shaded area: compressions, white area: dilatations) and P-wave polarity distribution (open circles: dilatations, full circles: compressions); E: focal mechanism obtained from the first significant peak of the reduced functions $m_{ij}(t)$, shown in Fig. 3B.

Fig. 4. A: Data (solid lines) and synthetic seismograms (dashed lines) obtained with the unconstrained inversion with the base functions constructed in the depth interval 0.5-1.9 km with spacing 0.2 km; data and synthetic seismograms are filtered at a cutoff frequency of 5 Hz and truncated with a D2 window with a duration of 5 s; B: $M_{ij}(t)$ functions (solid lines) obtained with the unconstrained inversion and reduced functions $m_{ij}(t)$ (dashed lines); C: joint time function constrained between 0 and 1, in the right upper part is indicated the scaling factor; D: average mechanism obtained from the six multipliers λ_{ij} associated with the joint time function of Fig. 4B.

Fig. 5. Inversion of waveforms of the event of November 8, 1986 (for more details see captions of Fig. 3). A: data (solid lines) and synthetic seismograms (dashed lines) obtained with the unconstrained inversion with the base functions constructed in the depth interval 0.5-1.9 km with the spacing of 0.2 km; data and synthetic seismograms are truncated with a D2 window with a duration of 10 s; B: $M_{ij}(t)$ functions (solid lines) obtained with the unconstrained inversion and reduced functions $m_{ij}(t)$ (dashed lines); C: joint time function constrained between 0 and 1, in the right upper part is indicated the scaling factor; D: average focal mechanism obtained from the six multipliers λ_{ij} and P-wave polarity distribution; E: focal mechanism obtained from the first significant peak of the reduced functions $m_{ij}(t)$ in Fig. 5B.

Fig. 6. A: Data (solid lines) and synthetic seismograms (dashed lines) obtained with the unconstrained inversion with the base functions constructed in the depth interval 0.5-1.9 km with spacing 0.2 km; data and synthetic seismograms are filtered at a cutoff frequency of 5 Hz and truncated with a D2 window with a duration of 10 s; B: $M_{ij}(t)$ functions (solid lines) obtained with the unconstrained inversion and reduced functions $m_{ij}(t)$ (dashed lines); C: joint time function constrained between 0 and 1. In the right upper part the scaling factor; D: average mechanism obtained from the six multipliers λ_{ij} associated with the joint time function of Fig. 16B.

Fig. 7. Inversion of waveforms of the event of November 8, 1986 (for more details see caption of Fig. 3). The V_p/V_s ratio used in the first 3.5 km of the extreme structures is around 2.1. A: data (solid lines) and

synthetic seismograms (dashed lines) obtained with the unconstrained inversion with the base functions constructed in the depth interval 0.5-1.9 km with spacing 0.2 km; data and synthetic seismograms are truncated with a D2 window with a duration of 5 s; B: $M_{ij}(t)$ functions (solid lines) obtained with the unconstrained inversion and the reduced functions $m_{ij}(t)$ (dashed lines); C: joint time function constrained between 0 and 1. In the right upper part the scaling factor is indicated; D: average focal mechanism obtained from the six multipliers λ_{ij} and P-wave polarity distribution; E: focal mechanism obtained from the first significant peak of the $m_{ij}(t)$ in Fig. 7B.

Fig. 8. Inversion of waveforms of the event of November 8, 1986 (for more details see captions of Fig. 3). The V_p/V_s ratio used in the first 3.5 km of the extreme structures is around 2.1. A: data (solid lines) and synthetic seismograms (dashed lines) obtained with the unconstrained inversion with the base functions constructed in the depth interval 0.5-1.9 km with the spacing of 0.2 km; data and synthetic seismograms are truncated with a D2 window with a duration of 10 s; B: $M_{ij}(t)$ functions (solid lines) obtained with the unconstrained inversion and the reduced functions $m_{ij}(t)$ (dashed lines); C: joint time function constrained between 0 and 1. In the right upper part the scaling factor is indicated; D: average focal mechanism obtained from the six multipliers λ_{ij} and P-wave polarity distribution; E: focal mechanism obtained from the first significant peak of the reduced $m_{ij}(t)$ functions, shown in Fig. 8B.

Fig. 9. Inversion of waveforms of the event of December 27, 1987 recorded, in Friuli, by 5 local stations (MPRV, BOOV, RCLV, BADV, ZOUV) respectively at epicentral distances of 8.7, 13.8, 26.3, 25.9 and 28.2 km, and azimuths of 145°, 83°, 232°, 107°, and 8°. Origin time: 00:21:01.55; epicentral coordinates: 46° 18.34'N, 12° 55.35'E. Data (solid lines) and synthetic seismograms (dashed lines) obtained with the unconstrained inversion with the base functions constructed in the depth interval 6-10 km with the spacing of 0.5 km; A: data and synthetic seismograms are truncated with a D2 window with a duration of 5.4 s centered around the dominant part of each signal; B: $M_{ij}(t)$ functions (solid lines) obtained with the unconstrained inversion and their reduced values $m_{ij}(t)$ (dashed lines); C: joint time function constrained between 0 and 1, in the right upper part is indicated the scaling factor; D: average

mechanism obtained from the six multipliers associated with the joint time function of Fig. 9C; E: mechanism obtained from the first peak of the reduced functions $m_{ij}(t)$.

Fig. 10. Inversion of waveforms of the event of December 27, 1987; data (solid lines) and synthetic seismograms (dashed lines) obtained with the unconstrained inversion with the base functions constructed in the depth interval 6-10 km with the spacing of 0.5 km; epicentral distances of 9.5, 14.7, 25.7, 26.9 and 28.1 km, and azimuths of 140°, 85°, 230°, 107°, and 10°. Origin time: 00:21:01.28; epicentral coordinates: 46° 18.44'N, 12° 54.59'E. A: data and synthetic seismograms are truncated with a D2 window with a duration of 5.4 s centered around the significant part of each signal; B: joint time function constrained between 0 and 1. In the right upper part is indicated the scaling factor; C: average mechanism obtained from the six multipliers associated with the joint time function of Fig. 10B; D: mechanism obtained from the first peak of the functions $m_{ij}(t)$.

Fig. 11. Data (solid lines) and synthetic seismograms (dashed lines) obtained with the unconstrained inversion with the base functions constructed in the depth interval 6-10 km with the spacing of 0.5 km; data and synthetic seismograms are filtered at a cutoff frequency of 5 Hz and truncated with a D2 window with a duration of 5.4 s; B: joint time function constrained between 0 and 1. In the right upper part is indicated the scaling factor; C: average mechanism obtained from the six multipliers λ_{ij} associated with the joint time function of Fig. 11B.

Fig. 12. Inversion of waveforms of the first event of February 1, 1988 recorded by four local stations (BUAV, BADV, PLRV, ZOUV); data (solid lines) and synthetic seismograms (dashed lines) obtained with the unconstrained inversion with the base functions constructed in the depth interval 2.5-5 km with the spacing of 0.5 km; epicentral distances of 19.4, 18, 17.8, and 23.7 km, and azimuths of 10°, 341°, 175°, and 141°. Origin time: 11:22:40.41; epicentral coordinates: 46 23.41'N, 13 09.98'E. A: data and synthetic seismograms are truncated with a D2 window with a duration of 6.9 s centered around the dominant part of each signal; B: $M_{ij}(t)$ functions (solid lines) obtained with the unconstrained inversion and the reduced functions $m_{ij}(t)$

(dashed lines); C: joint time function constrained between 0 and 1. In the right upper part is indicated the scaling factor; D:average mechanism obtained from the six multipliers associated with the joint time function of Fig. 12C; E: mechanism obtained from the first peak of the functions $m_{ij}(t)$.

Fig. 13. Data (solid lines) and synthetic seismograms (dashed lines) obtained from the first parametrization of the source with the unconstrained inversion. The base functions are constructed in the depth interval 2.5-5 km with the spacing of 0.5 km; data and synthetic seismograms are filtered with a cutoff frequency of 5 Hz and truncated with a D2 window with a duration of 6.9 s; B: $M_{ij}(t)$ functions (solid lines) obtained with the unconstrained inversion and the reduced functions $m_{ij}(t)$ (dashed lines); C: joint time function constrained between 0 and 1. In the right upper part is indicated the scaling factor; D: average mechanism obtained from the six multipliers λ_{ij} associated with the joint time function of Fig. 13C; E: mechanism obtained from the first peak of the reduced functions $m_{ij}(t)$.

Fig. 14. Data (solid lines) and synthetic seismograms (dashed lines) obtained from the second parametrization of the source with the unconstrained inversion. The base functions are constructed in the depth interval 2.5-5 km with the spacing of 0.5 km; data and synthetic seismograms are filtered with a cutoff frequency of 5 Hz and truncated with a D2 window with a duration of 6.9 s; B: $M_{ij}(t)$ functions (solid lines) obtained with the unconstrained inversion and the reduced functions $m_{ij}(t)$ (dashed lines); C: joint time function constrained between 0 and 1, in the right upper part the scaling factor is indicated; D: average mechanism obtained from the six multipliers λ_{ij} associated with the joint time function of Fig. 14C; E: mechanism obtained from the first peak of the reduced functions $m_{ij}(t)$.

Fig. 15. Inversion of waveforms of the second event of February 1, 1988 recorded by five local stations (BOOV, BUAV, BADV, PLRV, ZOUV) respectively at epicentral distances of 4.8, 15.5, 16.4, 21.4 and 24.9 km, and azimuths of 21°, 359°, 325°, 185° and 153° respectively. Origin time: 11:22:45.27; epicentral coordinates: 46° 21.14'N, 13° 06.61'E. Data (solid lines) and synthetic seismograms (dashed lines) obtained with the

unconstrained inversion with the base functions constructed in the depth interval 0.75-2 km with the spacing of 0.25 km; all base functions are constructed with the same extreme structural models (A and W). A: data and synthetic seismograms are truncated with a D2 window with a duration of 12 s centered around the dominant part of each signal; B: $M_{ij}(t)$ functions (solid lines) obtained with the unconstrained inversion and the reduced functions $m_{ij}(t)$ (dashed lines); C: joint time function constrained between 0 and 1, in the right upper part the scaling factor is indicated; D:average mechanism obtained from the six multipliers associated with the joint time function of Fig. 15C.

Fig. 16. Inversion of waveforms of the second event of February 1, 1988 recorded by 5 local stations (BOOV, BUAV, BADV, PLRV, ZOUV) respectively at epicentral distances of 4.8, 15.5, 16.4, 21.4 and 24.9 km, and azimuths of 21°, 359°, 325°, 185° and 153°; data (solid lines) and synthetic seismograms (dashed lines) obtained with the unconstrained inversion with the base functions constructed in the depth interval 0.75-2 km with the spacing of 0.25 km. The base functions relative to the station PLRV are respectively constructed with two extreme structural models A' and W' different from A and W. A: data and synthetic seismograms are truncated with a D2 window with a duration of 12 s centered around the dominant part of each signal; B: $M_{ij}(t)$ functions (solid lines) obtained with the unconstrained inversion and their reduced functions $m_{ij}(t)$ (dashed lines); C: joint time function constrained between 0 and 1, in the right upper part the scaling factor is indicated; D: average mechanism obtained from the six multipliers λ_{ij} associated with the joint time function of Fig. 16C.

Fig. 17. Data (solid lines) and synthetic seismograms (dashed lines) obtained with the unconstrained inversion with the base functions constructed in the depth interval 0.75-2 km with the spacing of 0.25 km; all the base functions are constructed with the same extreme structural models (A and W); data and synthetic seismograms are filtered with a cutoff frequency of 5 Hz and truncated with a D2 window with a duration of 12 s; B: $M_{ij}(t)$ functions (solid lines) obtained with the unconstrained inversion and their reduced functions $m_{ij}(t)$ (dashed lines); C: joint time function constrained between 0 and 1. In the right upper part the scaling factor is indicated; D: average mechanism

obtained from the six multipliers λ_{ij} associated with the joint time function of Fig. 17C; E: mechanism obtained from the first peak of the reduced functions $m_{ij}(t$.

Fig. 18. Data (solid lines) and synthetic seismograms (dashed lines) obtained with the unconstrained inversion with the base functions constructed in the depth interval 0.75-2 km with the spacing of 0.25 km; the base functions relative to the station PLRV are constructed with two extreme structural models A' and W' different from A and W; data and synthetic seismograms are filtered with a cutoff frequency of 5 Hz and truncated with a D2 window with a duration of 12 s; B: $M_{ij}(t)$ functions (solid lines) obtained with the unconstrained inversion and their reduced functions $m_{ij}(t)$ (dashed lines); C: joint time function constrained between 0 and 1, in the right upper part the scaling factor is indicated; D: average mechanism obtained from the six multipliers λ_{ij} associated with the joint time function of Fig. 18C; E: mechanism obtained from the first peak of the functions $m_{ij}(t)$.

TABLE I: Coordinates of the recording stations, origin time and hypocentral locations for the event of 11/08/1986, Pozzuoli area.

STATION	LATITUDE	LONGITUDE
ST07	40° 49.46'N	14° 04.41'E
ST08	40° 51.14'N	14° 05.87'E
ST11	40° 47.82'N	14° 09.64'E
ST13	40° 50.47'N	14° 08.29'E

ORIGIN TIME	LATITUDE	LONGITUDE	DEPTH	MODEL
04:20:48.16	40° 49.68'N	14° 05.52'E	1.1 km	POZZ1

TABLE II: Coordinates of the recording stations, origin times and hypocentral locations for the event of 12/27/1987, Friuli area.

STATION	LATITUDE	LONGITUDE
Monte Prat (MPRV)	46° 14.5'N	12° 59.3'E
Bordano (BOOV)	46° 19.2'N	13° 06.0'E
Montereale (RCLV)	46° 09.6'N	12° 39.2'E
Bernadia (BADV)	46° 14.2'N	13° 14.6'E
Zoufplan (ZOUV)	46° 33.4'N	12° 58.4'E

ORIGIN TIME	LATITUDE	LONGITUDE	DEPTH	MODEL
00:21:01.60	46° 18.24'N	12° 54.84'E	9.47	O.G.S.
00:21:01.28	46° 18.44'N	12° 54.59'E	9.64	FRIUL7A
00:21:01.55	46° 18.34'N	12° 55.35'E	7.13	FRIUL7W

TABLE III Coordinates of the recording stations, origin times and hypocentral locations for the first event of 2/1/1988, Friuli area.

STATION	LATITUDE	LONGITUDE
Buia (BUAV)	46° 13.1'N	13° 07.4'E
Bernadia (BADV)	46° 14.2'N	13° 14.6'E
Paularo (PLRV)	46° 33.0'N	13° 08.9'E
Zoufplan (ZOUV)	46° 33.4'N	12° 58.4'E

ORIGIN TIME	LATITUDE	LONGITUDE	DEPTH	MODEL
11:2_:41.30	46° 21.60'N	13° 05.40'E	5.1	O.G.S.
11:22:40.41	46° 23.41'N	13° 09.98'E	3.65	FRIUL7A
11:22:40.40	46° 23.39'N	13° 09,98'E	4.26	FRIUL7W

TABLE IV: Coordinates of the recording stations, origin times and hypocentral locations for the second event of 2/1/1988, Friuli area.

STATION	LATITUDE	LONGITUDE
Bordano (BOOV)	46° 19.2'N	13° 06.0'E
Buia (BUAV)	46° 13.1'N	13° 07.4'E
Bernadia (BADV)	46° 14.2'N	13° 14.6'E
Paularo (PLRV)	46° 33.0'N	13° 08.9'E
Zoufplan (ZOUV)	46° 33.4'N	12° 58.4'E

ORIGIN TIME	LATITUDE	LONGITUDE	DEPTH	MODEL
11:22:45.20	46° 21.80'N	13° 05.90'E	9.6	O.G.S.
11:22:45.27	46° 21.14'N	13° 06.61'E	1.33	FRIUL7A
11:22:45.27	46° 21.14'N	13° 06.60'E	1.46	FRIUL7W

TABLE V: Q values used in the extreme structures relative to the Pozzuoli area.

STRUCTURE POZZ1

THIKNESS OF THE LAYER (in km)	Q_S	Q_P
24.46	100	220
MANTLE	200	440

STRUCTURE POZZ2

THIKNESS OF THE LAYER (in km)	Q_S	Q_P
0.954	25	55
2.893	50	110
20.61	100	220
MANTLE	200	440

1B
38

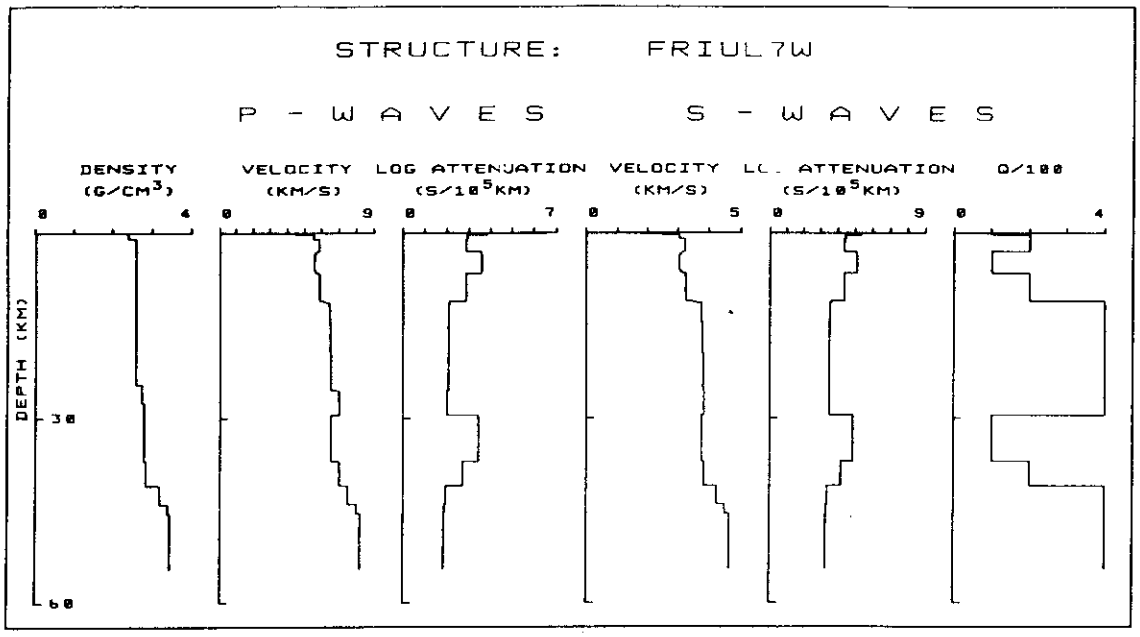
STRUCTURE: FRIUL7W
P - W A V E S
S - W A V E S
DENSITY (G/CM3)
VELOCITY (KM/S)
LOG ATTENUATION (S/10^5KM)
VELOCITY (KM/S)
LOG ATTENUATION (S/10^5KM)
Q/100
DEPTH (KM)
30
60

1A
37

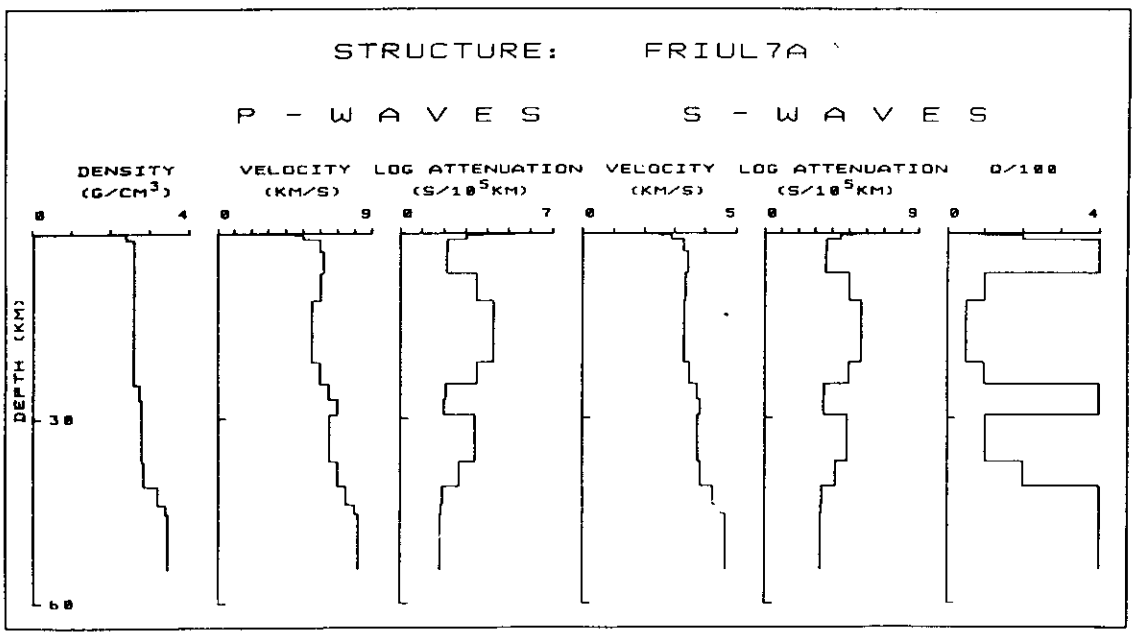
STRUCTURE: FRIUL7A
P - W A V E S
S - W A V E S
DENSITY (G/CM3)
VELOCITY (KM/S)
LOG ATTENUATION (S/10^5KM)
VELOCITY (KM/S)
LOG ATTENUATION (S/10^5KM)
Q/100
DEPTH (KM)
30
60

1D
40

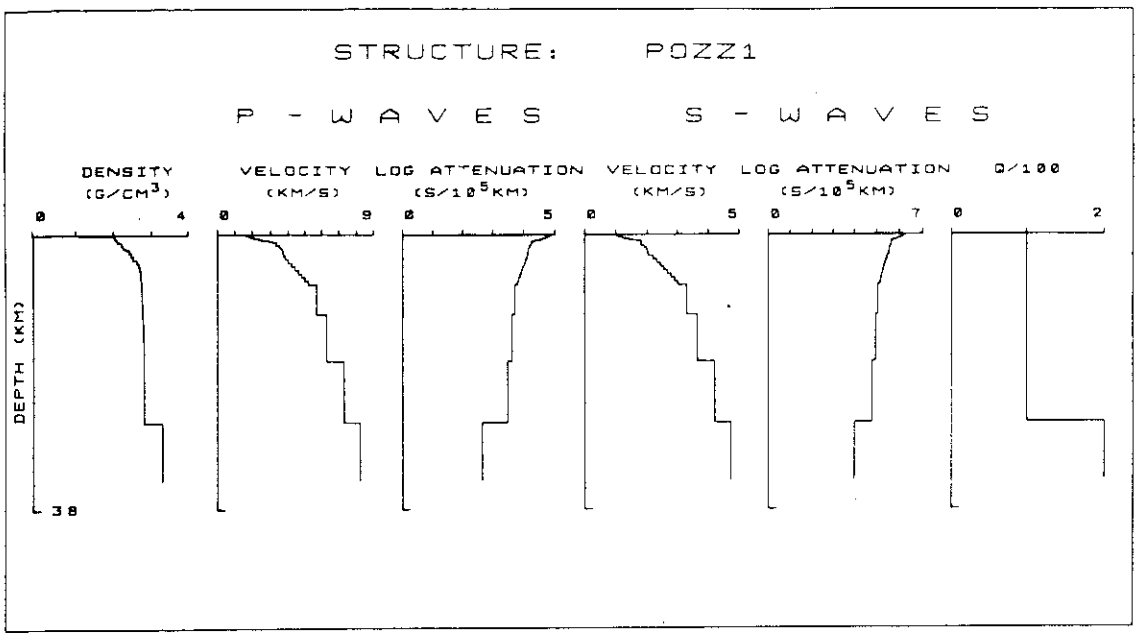
STRUCTURE: POZZ1
P - W A V E S
S - W A V E S
DENSITY (G/CM3)
VELOCITY (KM/S)
LOG ATTENUATION (S/10^5KM)
VELOCITY (KM/S)
LOG ATTENUATION (S/10^5KM)
Q/100
0
4
0
9
0
5
0
5
0
7
0
2
DEPTH (KM)
38

1C
39

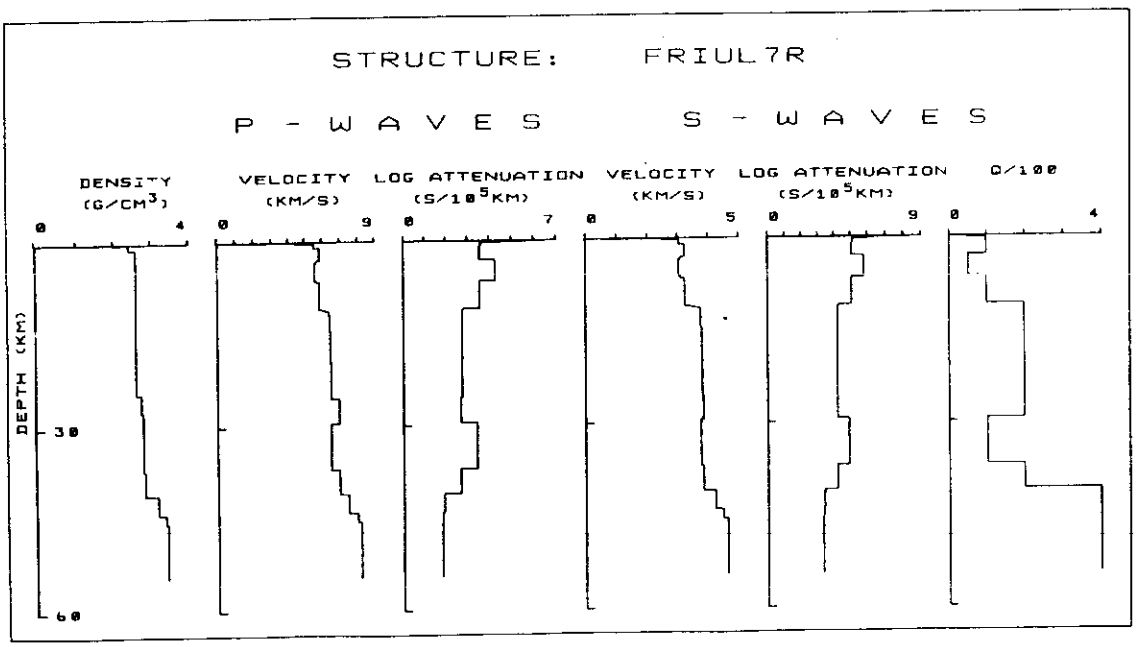
STRUCTURE: FRIUL7R
P - W A V E S
S - W A V E S
DENSITY (G/CM3)
VELOCITY (KM/S)
LOG ATTENUATION (S/10^5KM)
VELOCITY (KM/S)
LOG ATTENUATION (S/10^5KM)
Q/100
0
4
0
9
0
7
0
5
0
9
0
4
DEPTH (KM)
30
60

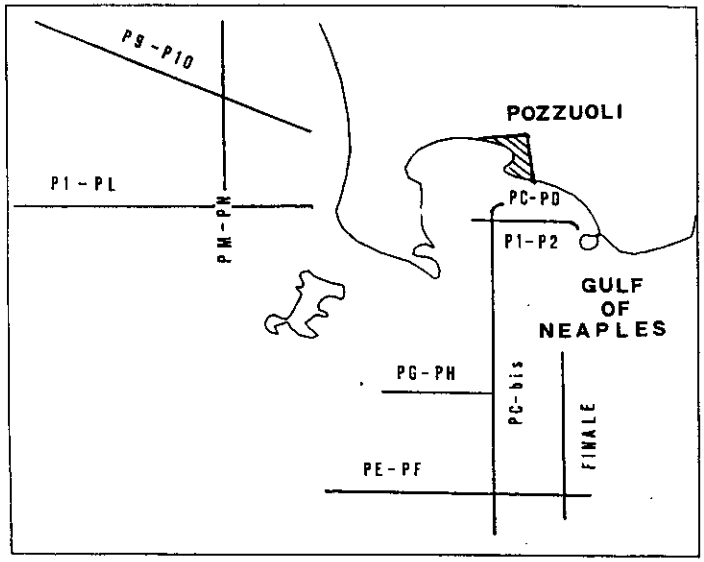

Map of the seismic lines recorded. Lines PC-PD, PC-bis, P1-P2, PC-PH and PE-PF: 24 folds (two S.P. every 25 m interval).

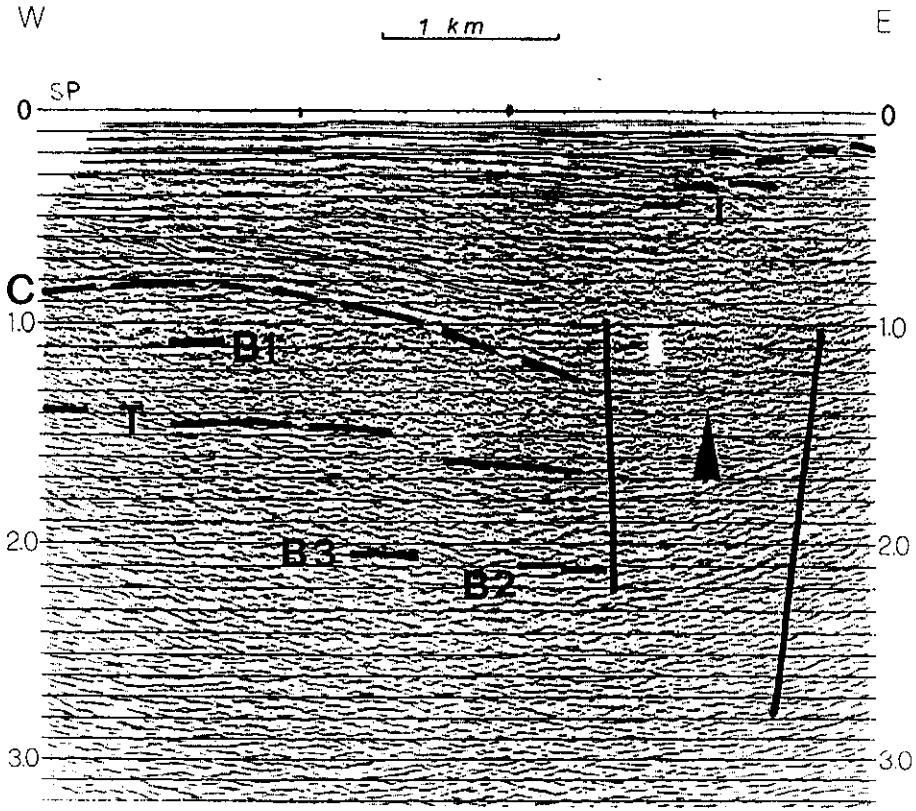

Migrated seismic section recorded in the gulf of Pozzuoli, E to W, 24 folds (P1-P2 line).
C = eventual top of the pre-caldera products, subaerial to submarine. I = lavas and hydrothermal products.
T = top of the thermometamorphic complex. B = trapped fluids, here not very clearly defined after migration of diffractions.
The arrow indicates the way of intrusion of the most recent volcanic products.

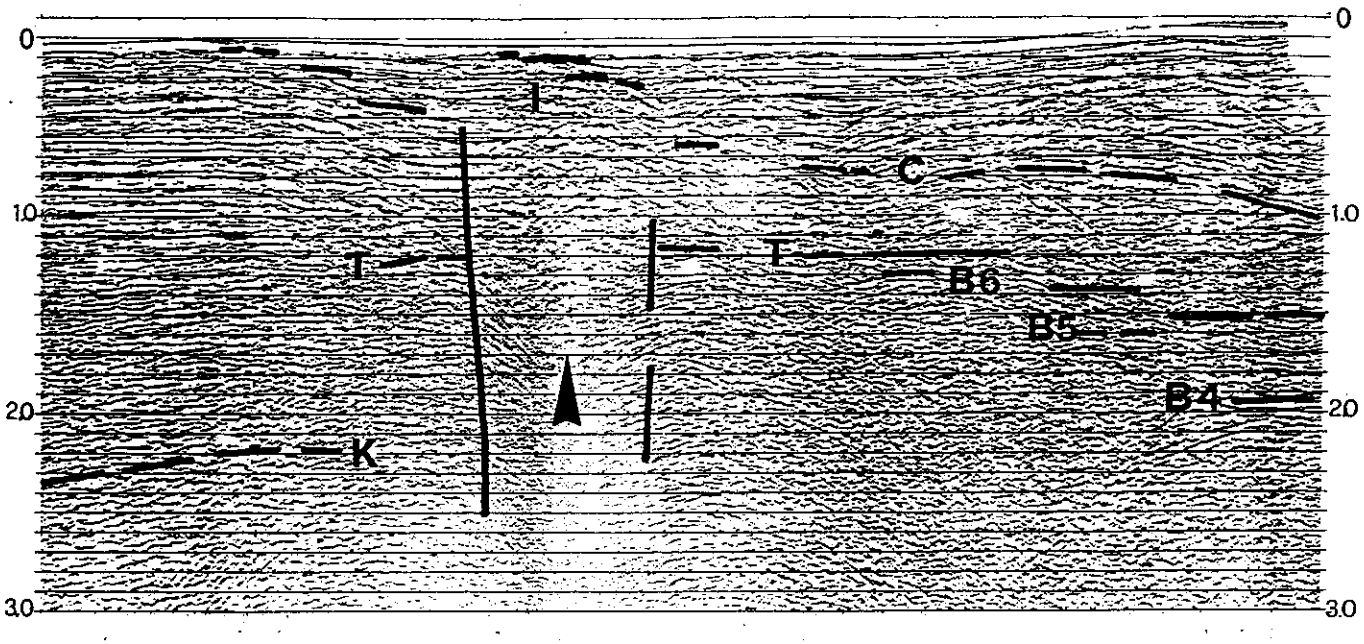

RAP seismic section recorded from Pozzuoli N to S, 24 folds (PC-PD line).
C = eventual top of the pre-caldera products, subaerial to submarine. I = lavas and hydrothermal products. T = top of the thermometamorphic complex. K = top of the carbonates. B = trapped fluids.
The arrow indicates the way of intrusion of the most recent volcanic products.

2C
43

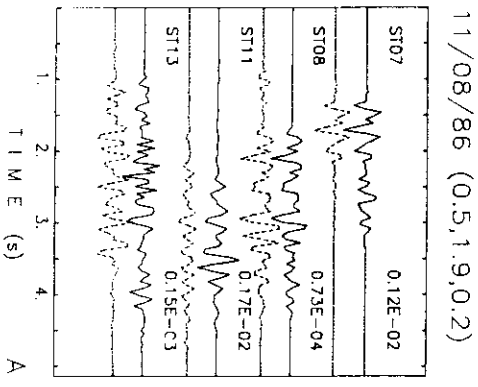

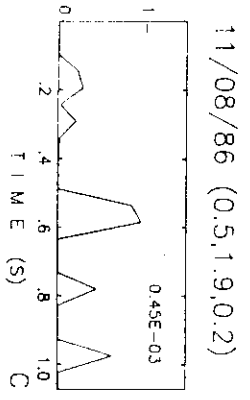

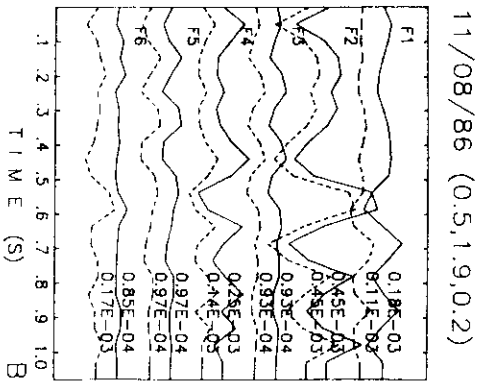

3
44

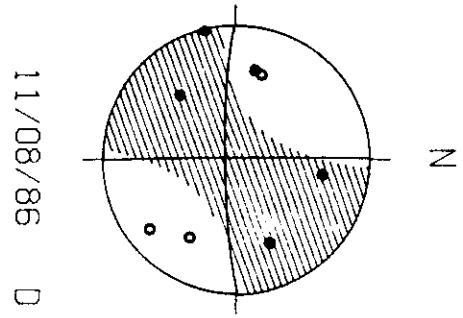
11/08/86 D
N

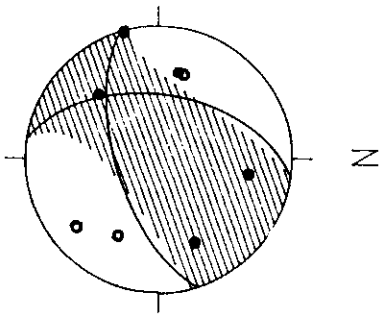
11/08/86 E
N

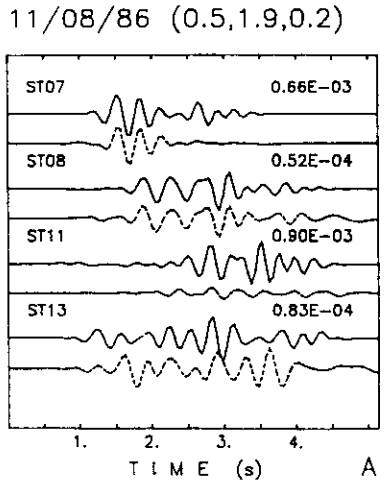
11/08/86 (0.5,1.9,0.2)
ST07
0.66E-03
ST08
0.52E-04
ST11
0.90E-03
ST13
0.83E-04
1.
2.
3.
4.
TIME (s)
A

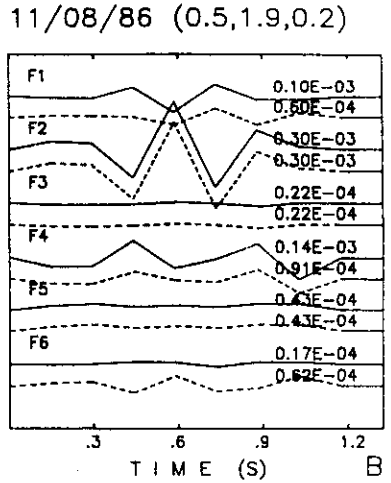
11/08/86 (0.5,1.9,0.2)
F1
0.10E-03
0.60E-04
F2
0.30E-03
0.30E-03
F3
0.22E-04
0.22E-04
F4
0.14E-03
0.91E-04
F5
0.43E-04
0.43E-04
F6
0.17E-04
0.62E-04
.3
.6
.9
1.2
TIME (S)
B

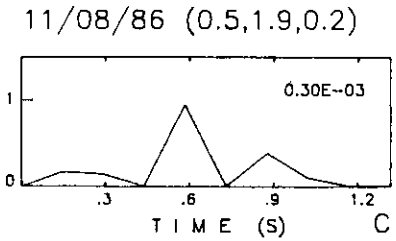
11/08/86 (0.5,1.9,0.2)
0.30E-03
1
0
.3
.6
.9
1.2
TIME (S)
C

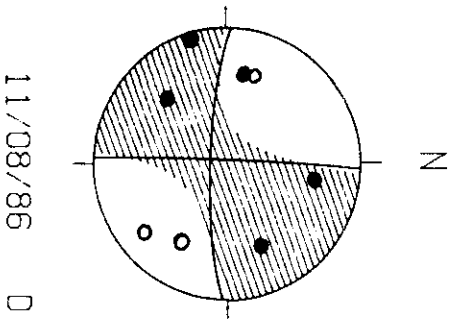
11/08/86 D
N

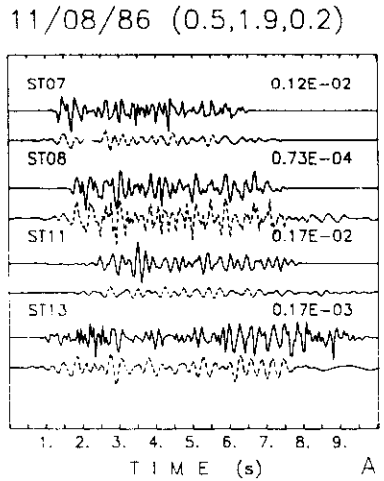
11/08/86 (0.5,1.9,0.2)
ST07
0.12E-02
ST08
0.73E-04
ST11
0.17E-02
ST13
0.17E-03
1. 2. 3. 4. 5. 6. 7. 8. 9.
TIME (s)
A

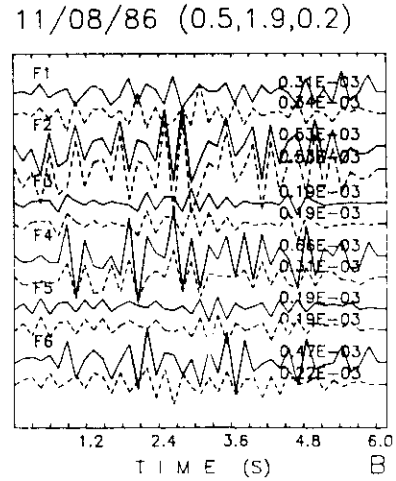
11/08/86 (0.5,1.9,0.2)
F1
F2
F3
F4
F5
F6
1.2 2.4 3.6 4.8 6.0
TIME (S)
B

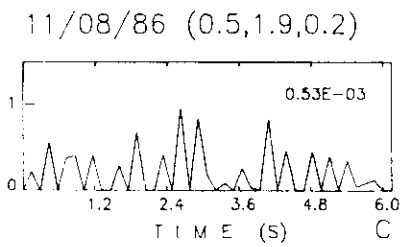
11/08/86 (0.5,1.9,0.2)
0.53E-03
1
0
1.2 2.4 3.6 4.8 6.0
TIME (S)
C

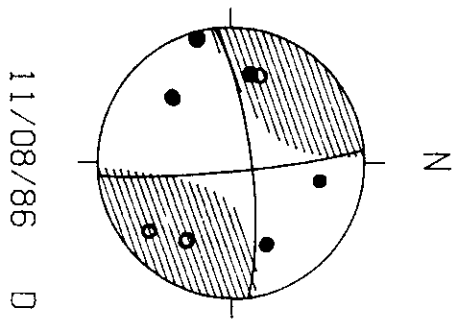
11/08/86 D
N

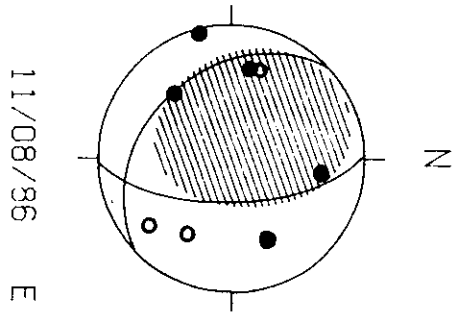
11/08/86 E
N

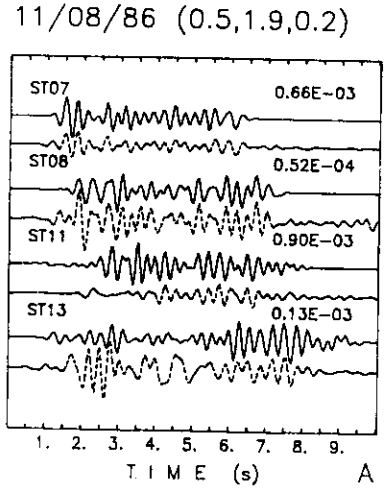
11/08/86 (0.5,1.9,0.2)
ST07
0.66E-03
ST08
0.52E-04
ST11
0.90E-03
ST13
0.13E-03
1. 2. 3. 4. 5. 6. 7. 8. 9.
TIME (s)
A

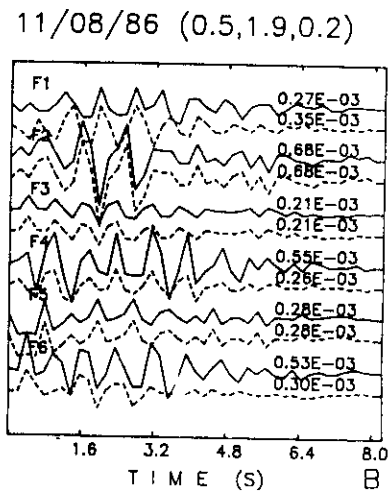
11/08/86 (0.5,1.9,0.2)
F1
0.27E-03
0.35E-03
F2
0.68E-03
0.68E-03
F3
0.21E-03
0.21E-03
F4
0.55E-03
0.26E-03
F5
0.28E-03
0.28E-03
F6
0.53E-03
0.30E-03
1.6 3.2 4.8 6.4 8.0
TIME (S)
B

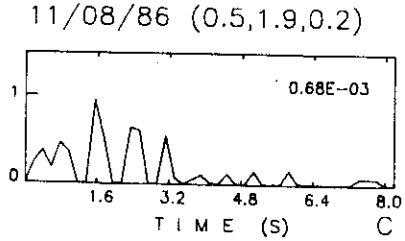
11/08/86 (0.5,1.9,0.2)
0.68E-03
1
0
1.6 3.2 4.8 6.4 8.0
TIME (S)
C

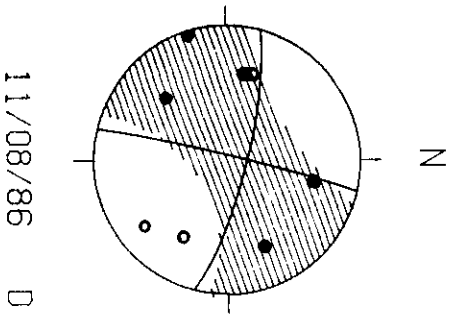
11/08/86 D
N

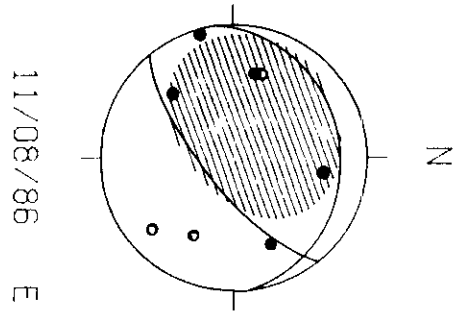
11/08/86 E
N

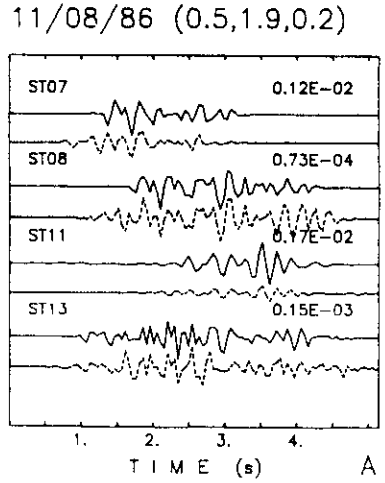
11/08/86 (0.5,1.9,0.2)
ST07
0.12E-02
ST08
0.73E-04
ST11
0.17E-02
ST13
0.15E-03
1.
2.
3.
4.
TIME (s)
A

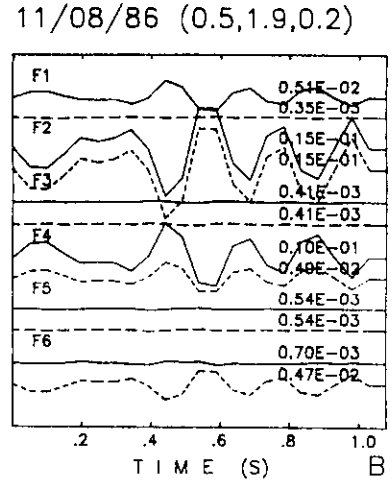
11/08/86 (0.5,1.9,0.2)
F1
0.51E-02
0.35E-03
F2
0.15E-01
0.15E-01
F3
0.41E-03
0.41E-03
F4
0.10E-01
0.49E-02
F5
0.54E-03
0.54E-03
F6
0.70E-03
0.47E-02
.2
.4
.6
.8
1.0
TIME (S)
B

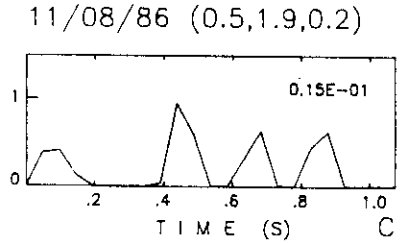
11/08/86 (0.5,1.9,0.2)
0.15E-01
1
0
.2
.4
.6
.8
1.0
TIME (S)
C

11/08/86 D

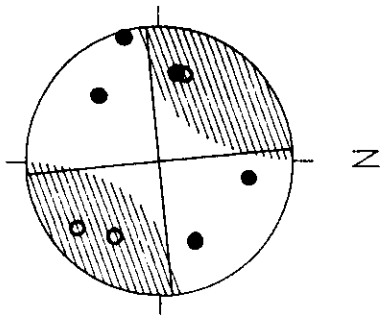

11/08/86 E

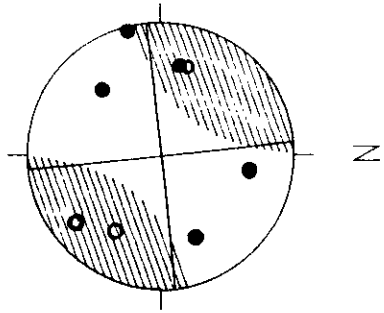

11/08/86 (0.5,1.9,0.2)

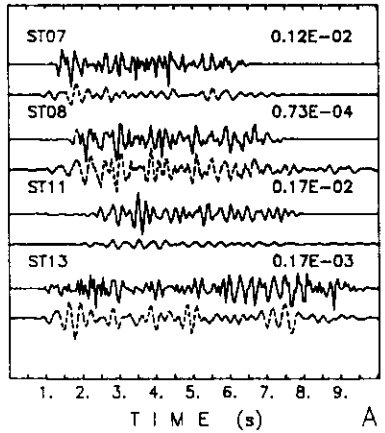

A

11/08/86 (0.5,1.9,0.2)

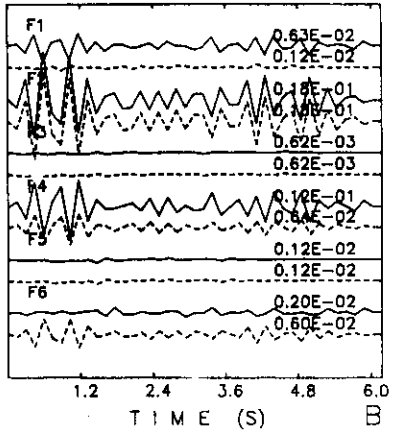

B

11/08/86 (0.5,1.9,0.2)

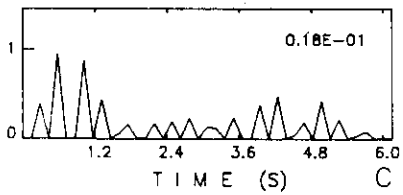

C

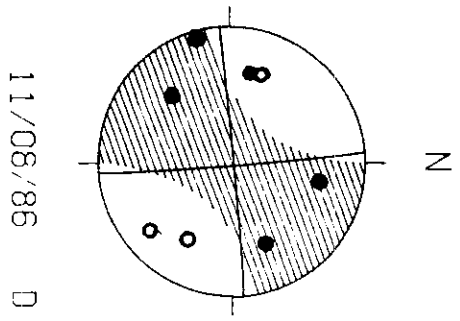
11/08/86 D
N

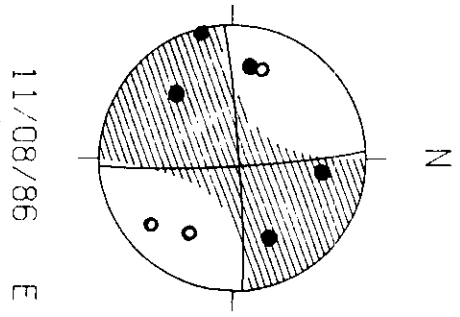
11/08/86 E
N

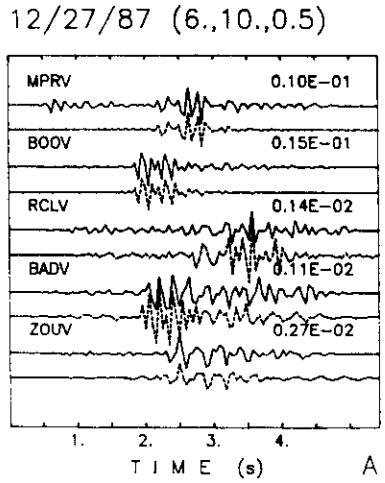
12/27/87 (6.,10.,0.5)
MPRV 0.10E-01
BOOV 0.15E-01
RCLV 0.14E-02
BADV 0.11E-02
ZOUV 0.27E-02
1. 2. 3. 4.
TIME (s)
A

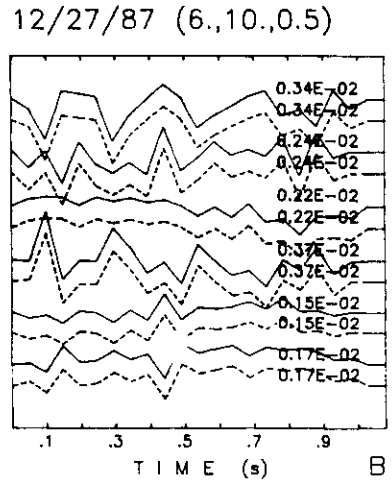
12/27/87 (6.,10.,0.5)
0.34E-02
0.34E-02
0.24E-02
0.24E-02
0.22E-02
0.22E-02
0.37E-02
0.37E-02
0.15E-02
0.15E-02
0.17E-02
0.17E-02
.1 .3 .5 .7 .9
TIME (s)
B

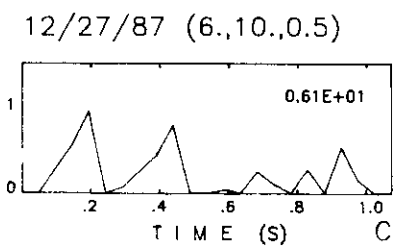
12/27/87 (6.,10.,0.5)
0.61E+01
1
0
.2 .4 .6 .8 1.0
TIME (S)
C

12/27/87 D
N
12/27/87 E
N

12/27/87 (6.,10.,0.5)
MPRV
0.10E-01
BOOV
0.15E-01
RCLV
0.14E-02
BADV
0.11E-02
ZOUV
0.27E-02
1.
2.
3.
4.
TIME (s)
A

12/27/87 (6.,10.,0.5)
0.37E-02
1
0
.2
.4
.6
.8
1.0
TIME (S)
B

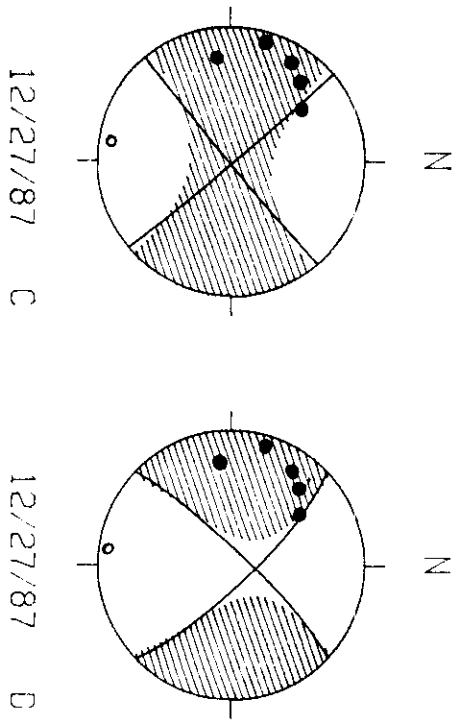
12/27/87 C
N
12/27/87 D
N

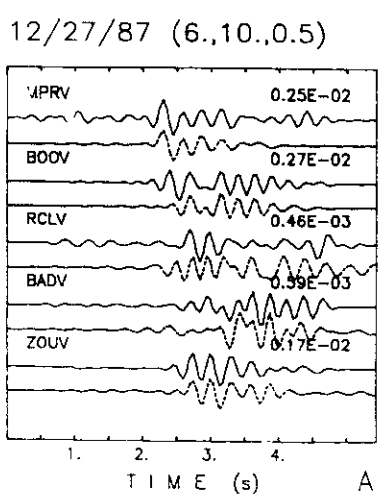
12/27/87 (6.,10.,0.5)
MPRV
0.25E-02
BOOV
0.27E-02
RCLV
0.46E-03
BADV
0.39E-03
ZOUV
0.17E-02
1.
2.
3.
4.
TIME (s)
A

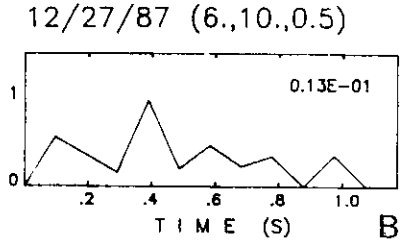
12/27/87 (6.,10.,0.5)
0.13E-01
1
0
.2
.4
.6
.8
1.0
TIME (S)
B

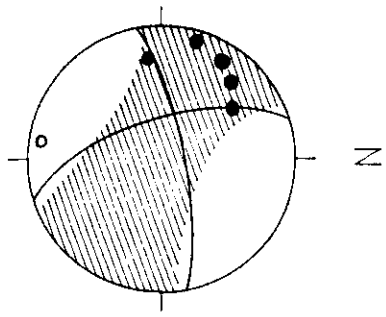
12/27/87
C
N

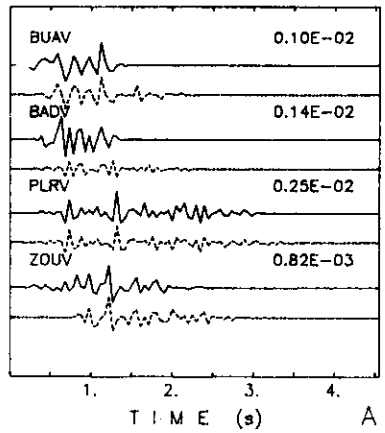
02/01/88 (2.5,5.,0.5) I
BUAV
0.10E-02
BADV
0.14E-02
PLRV
0.25E-02
ZOUV
0.82E-03
1.
2.
3.
4.
TIME (s)
A

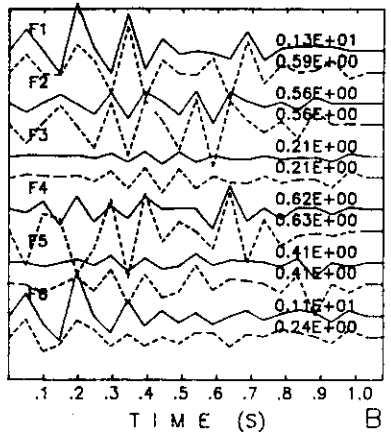
02/01/88 (2.5,5.,0.5) I
F1
F2
F3
F4
F5
F6
0.13E+01
0.59E+00
0.56E+00
0.56E+00
0.21E+00
0.21E+00
0.62E+00
0.63E+00
0.41E+00
0.41E+00
0.11E+01
0.24E+00
.1
.2
.3
.4
.5
.6
.7
.8
.9
1.0
TIME (S)
B

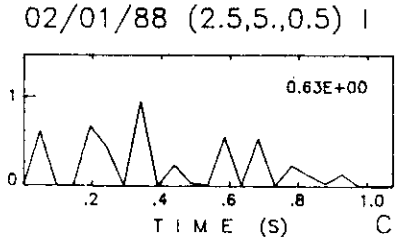
02/01/88 (2.5,5.,0.5) I
0.63E+00
1
0
.2
.4
.6
.8
1.0
TIME (S)
C

02/01/88 I D

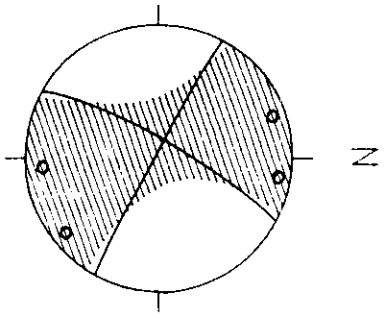

02/01/88 I E

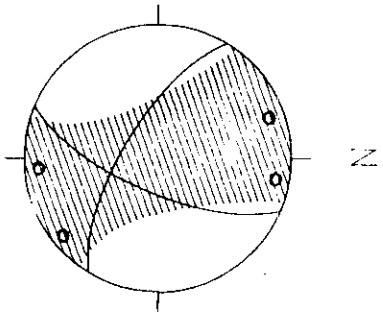

02/01/88 (2.5,5.,0.5) I

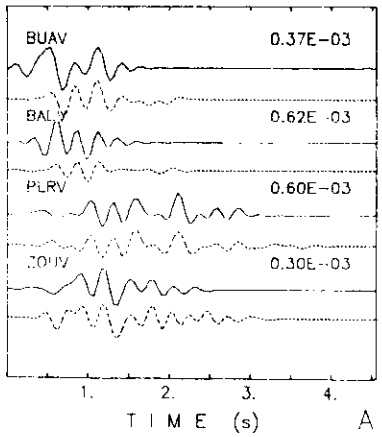

02/01/88 (2.5,5.,0.5) I

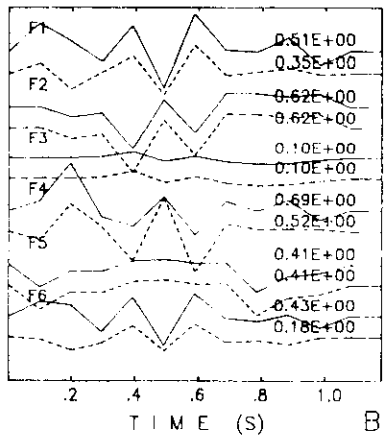

02/01/88 (2.5,5.,0.5) I

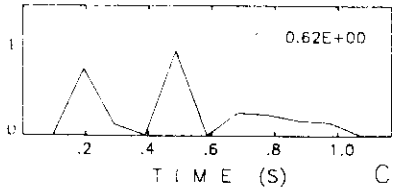

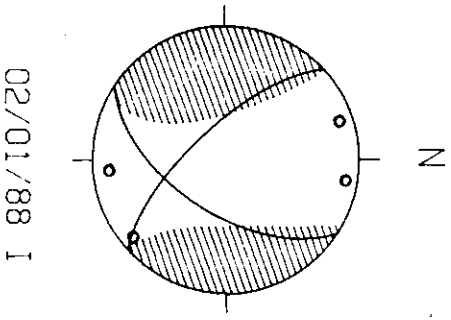

02/01/88 I D

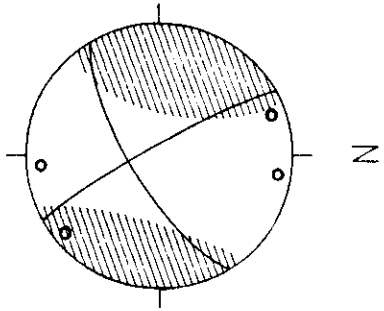

02/01/88 I E

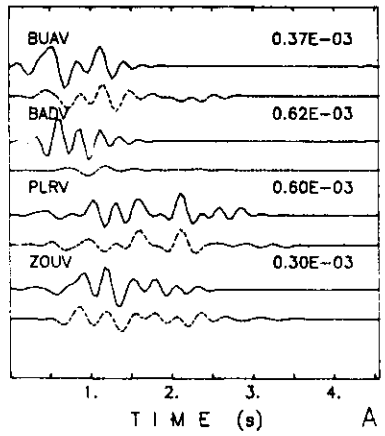

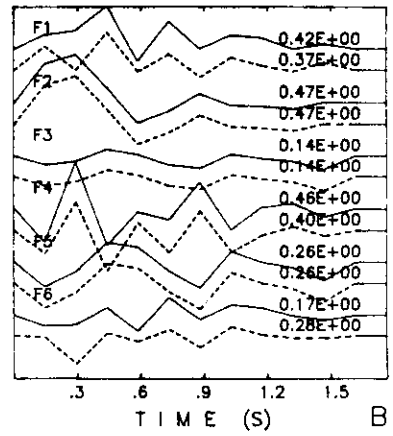

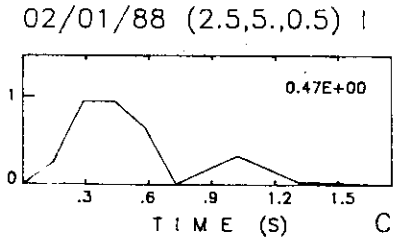

02/01/88 I D

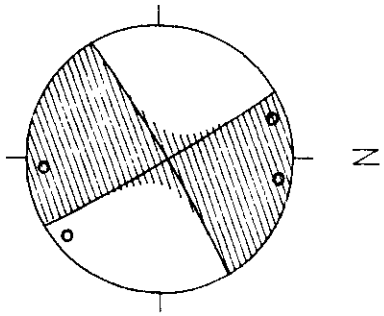

02/01/88 I E

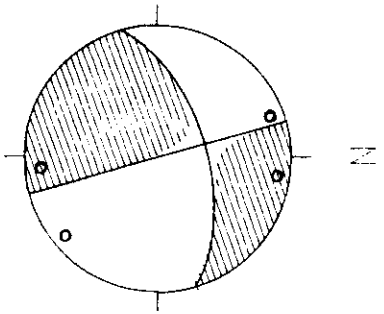

02/01/88 (0.75,2.,0.25) II

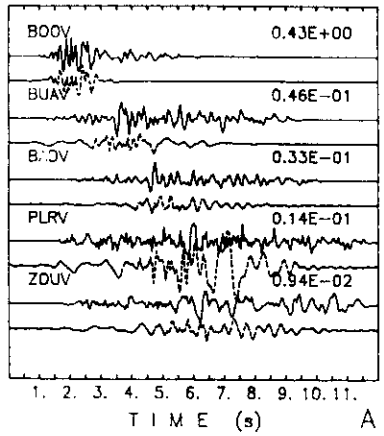

02/01/88 (0.75,2.,0.25) II

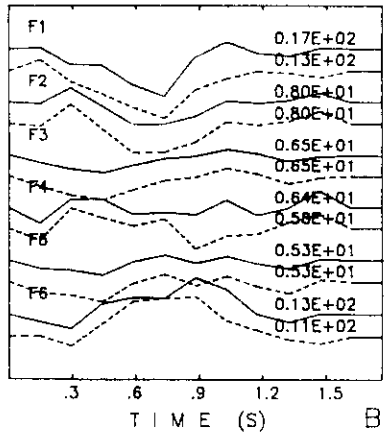

02/01/88 (0.75,2.,0.25) II

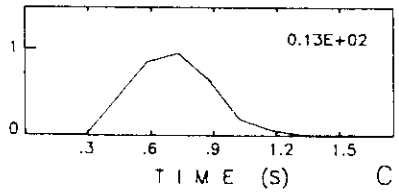

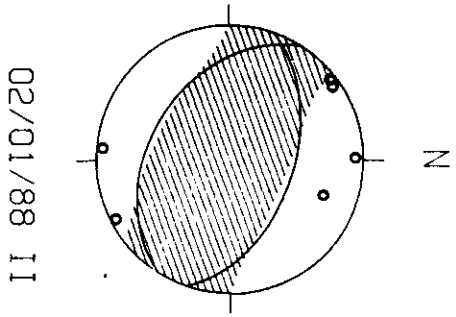

D II 88/01/20

02/01/88 (0.75,2.,0.25) II

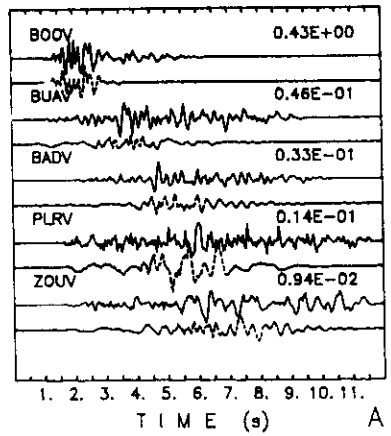

02/01/88 (0.75,2.,0.25) II

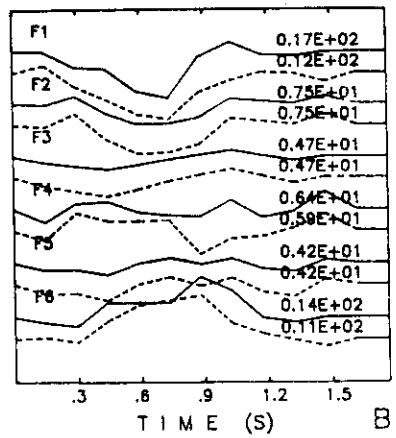

02/01/88 (0.75,2.,0.25) II

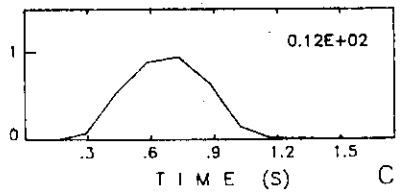

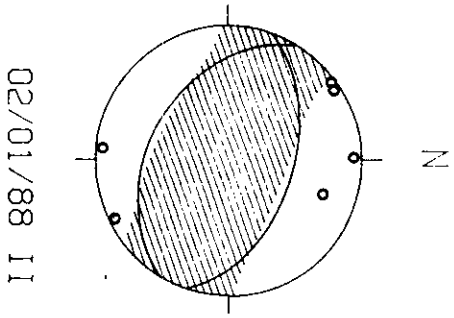
N

D II 88/10/20

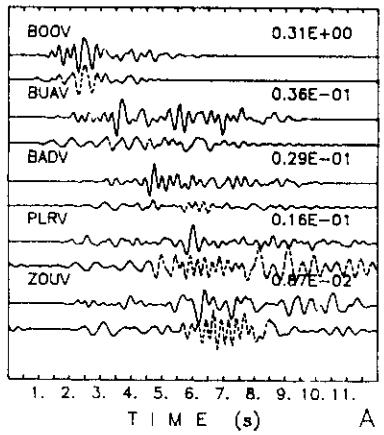
02/01/88 (0.75,2.,0.25) II
BOOV
0.31E+00
BUAV
0.36E-01
BADV
0.29E-01
PLRV
0.16E-01
ZOUV
0.87E-02
1. 2. 3. 4. 5. 6. 7. 8. 9. 10. 11.
TIME (s)
A

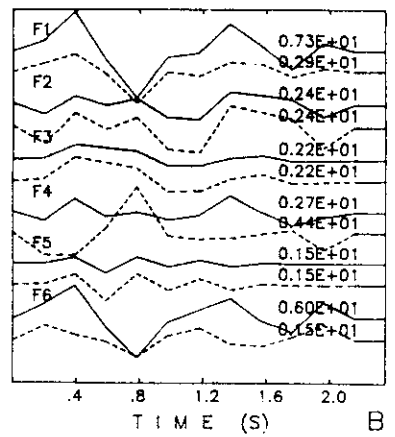
02/01/88 (0.75,2.,0.25) II
F1
0.73E+01
0.29E+01
F2
0.24E+01
0.24E+01
F3
0.22E+01
0.22E+01
F4
0.27E+01
0.44E+01
F5
0.15E+01
0.15E+01
F6
0.60E+01
0.15E+01
.4 .8 1.2 1.6 2.0
TIME (S)
B

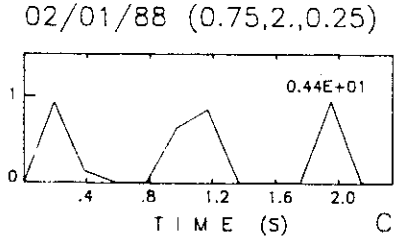
02/01/88 (0.75,2.,0.25) II
0.44E+01
1
0
.4 .8 1.2 1.6 2.0
TIME (S)
C

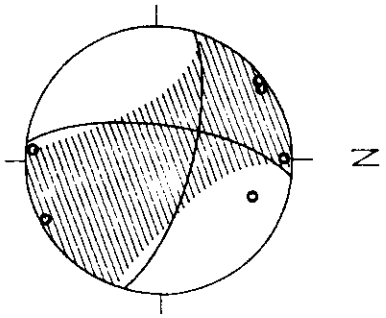

02/01/88 II D

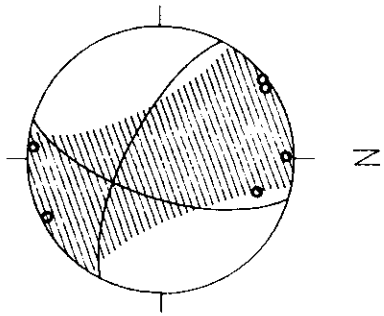

02/01/88 II E

02/01/88 (0.75,2.,0.25) II

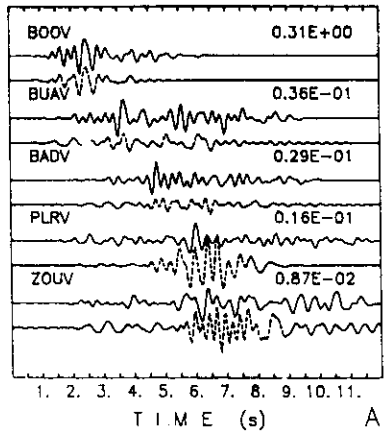

02/01/88 (0.75,2.,0.25) II

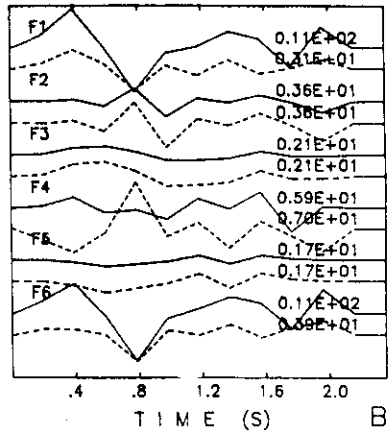

02/01/88 (0.75,2.,0.25) II

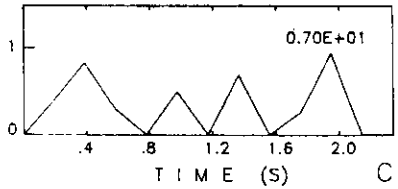

D 02/01/88 II
N

E 02/01/88 II
N